

Design and Integration of a Socket, Chamber, and Auto- mated Control System for an E-nose based on CMOS Pixe- lated Capacitive Sensor array

C.R. Chen
F. Lin
Electrical Engineering BSc
June 2025

Design and Integration of a Socket, Chamber, and Automated Control System for an E-nose based on CMOS Pixelated Capacitive Sensor array

by

C.R. Chen
F. Lin

to obtain the degree of Bachelor of Science
at the Delft University of Technology.

Student number:	C. R. Chen	5677556
	F. Lin	5599784
Project duration:	April 21, 2025 – June 27, 2025	
Supervisors:	Prof. dr. ir. F.P. Widdershoven,	TU Delft, NXP Semiconductors
	MSc. T. Shen	TU Delft
	Dr. M. Kabatas	TU Delft
Thesis committee:	Prof. dr. ir. F.P. Widdershoven,	TU Delft, NXP Semiconductors
	MSc. T. Shen	TU Delft
	Dr.ir. C.J.M. Verhoeven	TU Delft

An electronic version of this thesis is available at <http://repository.tudelft.nl/>.

Abstract

This thesis presents the design and implementation of a socket, a chamber and an automated control system for an electronic nose (e-nose) based on CMOS Pixelated Capacitive Sensor (PCS) array chip in a Quad Flat No-Leads (QFN) 5 mm x 5 mm chip package. The objective of this project is to enable repeatable and reliable detection of volatile organic compounds (VOCs) by ensuring a gas-tight sensing environment and minimizing human intervention in experimental procedures, while ensuring good electrical connections by the socket.

A socket was developed to ensure good electrical contact using an anisotropic conductive sheet, allowing the QFN-packaged PCS chip to be inserted and removed without the need for soldering. The socket interfaces with a tightly sealed chamber to prevent gas leakage (< 0.1 ml/min) and maintain a stable gas flow across the sensor. Both components were prototyped in Polyethylene Terephthalate Glycol (PETG) and therefore do not fulfill the final requirement for heat and chemical resistance yet.

To automate gas delivery, the system integrates Bronkhorst mass flow controllers and RVM industrial microfluidic rotary valves. A Python-based graphical user interface (GUI) was developed to schedule gas flow profiles, control valve positions and compute VOC concentrations using the Antoine equation and Dalton's Law of Partial Pressures. This enables dynamic delivery of programmable VOC concentration. Although the automated control system meets most mandatory requirements and all trade-off requirements, some limitations remain. These include unreliable serial communication with the valve during automated operation, even though manual operation through the GUI is executed reliably. This inconsistency is likely caused by timing or firmware-related issues.

Preface

This thesis is written for the Bachelor Graduation Project Electrical Engineering at Delft University of Technology. The project is carried out by three subgroups, each with two members, to come to a final product at the end: a fully automated e-nose prototype. During this project, the subgroups have worked together, offering support and exchanging ideas when needed, which greatly enriched the process and the outcome.

Firstly, we want to thank our supervisors, Prof. dr. ir. F.P. Widdershoven, Mr. T. Shen and Dr. M. Kabatas, for their support, guidance and encouragement throughout this project. We are truly grateful for the time, insight, and dedication they invested in our work. Additionally, we want to thank Delft University of Technology for the knowledge obtained in the past three years and for providing the resources and environment that made this project possible. We also want to thank NXP Semiconductors for supplying the functionalized CMOS chips in a QFN package, which enabled us to carry out our work effectively. Lastly, we want to express our gratitude to the members of the other subgroups: Yousri Machtane, Pieter Olyslaegers, Kevin Pang, and Wilson Rong, for their dedication, collaboration, and support throughout this project.

*C.R. Chen
F. Lin
Delft, June 2025*

Contents

1	Introduction	1
1.1	State of the Art	1
1.1.1	Socket.	1
1.1.2	Chamber	1
1.1.3	Microfluidic Gas Supply System	2
1.2	Problem Definition	2
1.3	Project Goals and Scope.	2
1.4	Thesis Outline	3
2	Background Information	4
2.1	E-nose	4
2.1.1	Chip Package.	4
2.2	Gas Sensing Setup.	5
3	Programme of Requirements	7
4	Design	9
4.1	Shared Design Considerations Between the Socket and the Chamber	9
4.1.1	Material Properties	9
4.1.2	Production Constraints	10
4.1.3	Final Material Selection	10
4.2	Socket.	10
4.2.1	Socket-PCB Connection	11
4.2.2	Anisotropic Conductive Sheet	12
4.3	Adapter PCB	12
4.3.1	Adapter PCB Layout	13
4.4	Chamber	14
4.4.1	Gas In- and Outlet	14
4.4.2	Chamber Socket Connection	15
4.4.3	Square Support Frame.	16
4.5	Automated Control System	16
4.5.1	Bronkhorst Mass Flow Controller - FLEXI-FLOW.	17
4.5.2	The Digital Chilling/Heating Dry Bath	18
4.5.3	RVM Industrial Microfluidic Rotary Valve - FAST Model	18
4.5.4	Graphical User Interface	19
5	Results	21
5.1	Socket.	21
5.2	Chamber	22
5.3	Automated Control System	22
5.3.1	Valve Position Setup	22
5.3.2	Graphical User Interface	23
6	Discussion	28
6.1	Socket.	28
6.2	Chamber	28
6.3	Automated control system	29
7	Conclusion	30
7.1	Recommendations and Future Work	30

A	Technical drawings	32
A.1	QFN MLPX5-24-OP01 Package	32
A.2	Socket	33
A.2.1	Barbed Rivets	34
A.3	Chamber	34
A.4	C-shaped Slider	35
B	Socket-PCB connection considerations	36
B.1	Usage of Rubber	36
B.2	Press-fit	36
B.3	Snap Ring	37
C	Chamber-Socket connection considerations	38
C.1	Clamping Mechanisms	38
C.2	Socket-PCB-Based Fixation	38
D	Flow Characterization in Tubes	39
D.1	Reynolds Number	39
D.2	Taylor Dispersion	40
E	VOC Concentration Calculations	41
E.1	Flow Rate Equation for Setpoint Concentration	41
E.2	Error Margin	42
E.3	Antoine Coefficients	43
F	3D Rendering of the Adapter PCB Setup	44
G	The Experimental Setup	45
G.1	Valve	45
G.2	Chamber	45

Introduction

Food spoilage leads to economic losses and health risks, which is a challenge for both the food and agricultural industries. An electronic nose (e-nose) offers a solution for this problem by detecting gases released during spoilage. This device mimics the human sense of smell but is also capable of detecting odors and gases that are imperceptible to the human nose, such as carbon monoxide. It typically includes a gas sensor array, a transmission path for gases, a microprocessor, and an identification method to interpret the data. E-noses have been widely used in several fields, such as food, health, environmental, and security sectors [1].

The type of e-nose that is used in this project is based on complementary metal oxide semiconductor (CMOS) technology, which has a low cost and is energy efficient. The system employs CMOS Pixelated Capacitive Sensor (PCS) array chip and is functionalized by printing sensing ink on a PCS array by inkjet printing. This sensing ink is an inkjet-printable material with dielectric properties that can be modulated by external stimuli. With the CMOS PCS array chip, the presence and type of volatile organic compounds (VOC) can be determined, which are carbon-based chemicals that easily evaporate at room temperature. To assess and compare the selectivity and sensitivity of different sensing inks under exposure to a specific VOC, measurements must be performed repeatedly under the same conditions. To evaluate the performance of the e-nose in detecting different gases, it is essential to perform repetitive experiments. To enable this, the project focuses on designing a custom chip socket and gas chamber to ensure stable and accurate positioning of the PCS chip during exposure to different gases, as well as an automated control system to deliver precise gas mixtures.

1.1. State of the Art

1.1.1. Socket

Currently, there are sockets, such as clamshell and zero-insertion-force (ZIF), that are essential for testing integrated circuits like Ball Grid Array (BGA) and Quad Flat No-lead (QFN) packages. As outlined by Ironwood Electronics [2], clamshell sockets utilize spring pins to achieve low contact resistance ($< 30\text{m}\Omega$). Furthermore, they support high-frequency operation ($> 40\text{GHz}$) and ensure uniform pressure distribution across the package. ZIF sockets, on the other hand, allow insertion and removal without applying mechanical force. This makes them suitable for repeated testing. Moreover, these sockets provide excellent signal integrity with low signal loss (1 dB at 6.5 GHz). While these technologies have high performance, the socket design for the PCS chip used in this project focuses on repeated use, precise alignment with the chip and minimal socket dimensions.

1.1.2. Chamber

Chambers are commonly used in e-nose systems. For example, Borowik et al. [3] designed an e-nose system to detect the fungus *Ciboria batschiana* with an open sensor chamber with a sliding shutter. This design allowed the sensor to be directly exposed to the small volumes of sample air, enabling accurate detection of the odor compounds without dilution. Xu et al. [4] designed a chamber with a hemispherical design for their e-nose system to detect the citrus green disease Huanglongbing (HLB)

at different stages of infection, to reduce turbulence and improve the stability of the gas flow. This design also reduced the cleaning dead space that may occur during the gas flow. Samiyan et al. [5] compared the performance of hemispherical, rectangular, and cylindrical chambers using gas flow simulations. The hemispherical chamber had a smaller stagnant region and a larger gas-to-sensor contact area compared to rectangular and cylindrical chambers. While these studies demonstrate how the geometric design can enhance gas flow uniformity and sensor performance, the chamber design for the PCS chip used in this project takes a different approach. The gas-to-sensor contact area is always limited to the surface of the chip area and does not depend on the shape of the chamber. However, the volume of the chamber should still be minimized to reduce the gas refresh time and maximize the gas concentration inside the chamber.

1.1.3. Microfluidic Gas Supply System

Microfluidic gas supply systems are often used to introduce gases into a chamber that can hold multiple sensors. In the design of the e-nose system of Xu et al. [4] the sensor response mechanism of HLB-specific VOCs was investigated. A microfluidic gas supply system for HLB was designed by using a thermostat and positive-temperature-coefficient (PTC) heater to heat and precisely control the chamber temperature. To ensure stable gas flow, the system also integrated a micro vacuum pump in combination with a precision gas flow stabilizer valve and a glass rotor flow meter.

Another example of an e-nose system that uses a microfluidic gas supply system was developed by Wu et al. [6], which has 37 metal oxide sensors to detect 14 odors at varying concentrations. Their sensing setup ensures a stable and controlled sample environment to detect various odors. The setup consists of mass flow controllers and solenoid valves to automatically switch between multiple gas inlet pathways. To minimize the effect of temperature fluctuations, the sensors were housed in a thermostatically controlled chamber.

In this project, a microfluidic gas supply system is also used to create a stable environment for testing multiple chemicals at varying concentrations. However, a digital chilling/heating dry bath is used to stabilize the temperature. Furthermore, mass flow controllers are used to regulate the flow rates and rotary valves are used to switch the flow paths.

1.2. Problem Definition

To miniaturize the system, a PCS chip is now mounted on a 5 mm x 5 mm quad flat no-lead (QFN) package instead of the much larger 24-pin CDIL package used in a former system. Consequently, the socket of the former system is incompatible with the smaller QFN packages.

In addition to the socket and chamber incompatibility, the existing microfluidic gas supply system operates entirely manually. This setup is time-consuming, requires constant supervision, and is prone to human errors. A detailed description of the conventional setup and its shortcomings is provided in section 2.2. To overcome these issues, the gas control system should be modernized with new equipment and should have a clear graphical user interface (GUI) for easy operation.

Therefore, the problem definition of the thesis is the following: *"The socket and the chamber should be gas-tight and provide good electrical connections with a QFN-packaged PCS chip, while the gas sensing setup should be automated to minimize manual intervention and improve experimental reliability."*

1.3. Project Goals and Scope

This thesis addresses the aforementioned challenges by developing three key components:

1. Design and realization of a gas-tight chip socket that matches precisely the QFN MLP5X5-24-OP01 chip package (5mm × 5mm, 24 leads) and that consistently makes good contact with the chip. It shall allow easy insertion and removal of the chip package from the PCB. It shall also be heat- and chemically resistant to prevent deformation due to temperature variations and material degradation due to VOC exposure.
2. Design and realization of a gas chamber that can be assembled with the socket, while ensuring

a closed environment around the chip package. It shall also be heat- and chemically resistant to prevent deformation and material degradation resulting from temperature variation and exposure to VOCs.

3. Developing an automated system for a microfluidic gas supply system consisting of multiple Bronkhorst FLEXI-FLOW™ compact mass flow controllers (MFC) and multiple RVM industrial microfluidic rotary valves, including a graphical user interface (GUI).

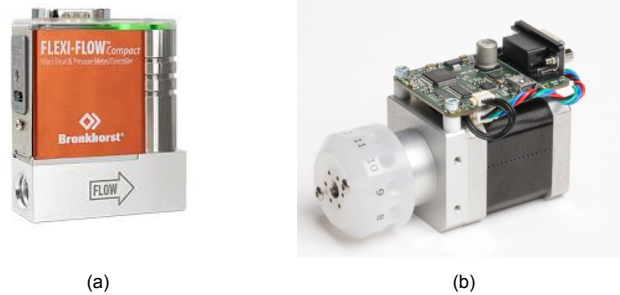


Figure 1.1: Overview of the used devices in the automated control system: **(a)** Bronkhorst mass flow controller - Flexi Flow, **(b)** RVM industrial microfluidic rotary valve

1.4. Thesis Outline

This thesis consists of seven chapters. Chapter 2 provides background information on the project. Chapter 3 outlines the mandatory and trade-off requirements that the socket, chamber, and automated control system must fulfill. Chapter 4 presents the design and considerations for the socket, the chamber, and the automated control system. The results will be presented in Chapter 5 and discussed in Chapter 6. Chapter 7 provides the conclusion of this project and suggestions for future work.

2

Background Information

2.1. E-nose

The e-nose in this project uses a CMOS Pixelated Capacitive Sensor (PCS) array chip. Sensing inks will be printed on a PCS array using inkjet printing. With the sensors, the presence and type of VOC can be determined as follows. In the situation when there is no VOC interaction with the sensing ink, the capacitance of the sensing ink is used as a baseline, Figure 2.1. When the VOCs interact with the sensing ink, the ink absorbs the VOC molecules, Figure 2.2. This will result in a change of the relative permittivity ϵ_r of the sensing ink, causing a change in capacitance, as described by the equation:

$$C = \frac{\epsilon_0 \epsilon_r A}{d} \quad (2.1)$$

where

- ϵ_0 is the permittivity of the vacuum, which is 8.854×10^{-12} F/m
- ϵ_r is the relative permittivity of the sensing ink
- A is the surface area of the electrodes in m^2
- d is the distance between the electrodes in m

By comparing the capacitance before and after VOC exposure, the system can detect the presence of the VOC. To measure at specific locations in the sensor array, a specific sense capacitor can be selected by toggling the potential of its active electrode while grounding the adjacent electrodes. This configuration allows the PCS chip to detect and measure the capacitance at that particular sensing location [7].

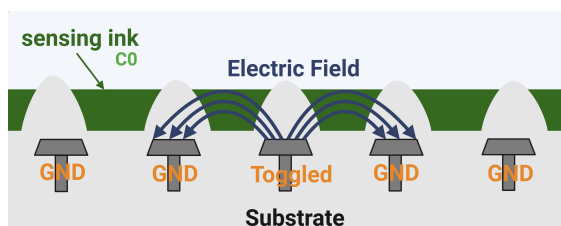


Figure 2.1: Row of sense electrodes with sensing ink without interaction with VOC

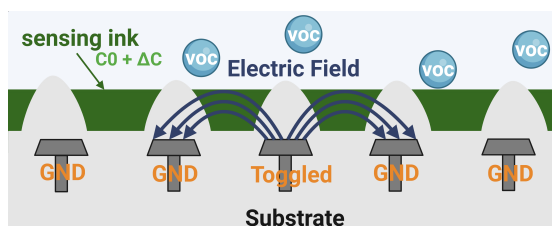


Figure 2.2: Row of sense electrodes with sensing ink with interaction with VOC

2.1.1. Chip Package

To protect the PCS chip against physical damage, moisture, and dust, a chip package is used. The package also enhances the longevity and performance, making it more reliable in diverse operating conditions [8].

In this project, the quad flat no-lead (QFN) MLP5X5-20-OP-01 open-cavity chip package from Sempac is used, which has 24 leads and dimensions of 5 mm x 5 mm [9]. Compared to the previously used chip package, this is a smaller package, which makes the overall system more compact. The drawings of the QFN package used in this project are shown in section A.1.

The QFN package has electrode contacts along all four sides instead of leads. This allows for a reduction of the mounting area and lowers the height in comparison with the previously used QFP packages. The open cavity version of the QFN packages allows the PCS array to be exposed to VOCs. This exposure is necessary for the sensor's operation, but significantly increases the fragility of the packaged chip. The exposed sensing areas and the printed sensing inks are vulnerable to physical damage. Therefore, the socket should ensure that the QFN package can be inserted and removed without any contact with these exposed parts.

2.2. Gas Sensing Setup

A gas sensing setup was used to expose the PCS chip to VOCs, allowing the sensing ink on the chip to interact with the VOCs. The PCS chip is placed in a socket that is enclosed within a gas chamber. VOCs are introduced into the chamber by inserting inlet tube and directing the gases through them. The conventional gas sensing setup uses syringe pumps, ice baths, and mechanical valves, as shown in Figure 2.3.

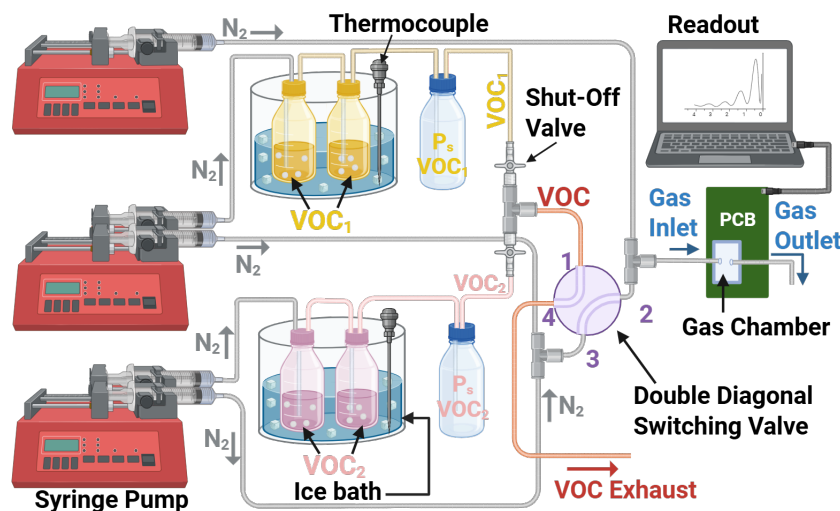


Figure 2.3: Conventional gas sensing setup

The syringe pumps on the left side of the figure pump nitrogen through bottles containing VOCs. The VOCs used in the lab include 2-nonanol, nonanal, tetradecane, 1-dodecanethiol, ethanol, 1-propanol, 2-propanol, methanol, acetone, α -pinene, α -terpinene, 1-butanol, toluene and 2-butanone (MEK). Although the conventional gas sensing setup is functional, it has several limitations that affect both the measurement quality and the convenience of the experiment. The setup requires manual operation at nearly every step:

- The flow rate of each syringe pump has to be set manually.
- The limited volume of the syringes requires frequent refilling.
- The VOC bottles are placed in an ice bath to reach the desired temperature. A temperature sensor must be placed in the second bubble bottle in the ice bath to check the temperature.
- Switching between different flow paths (mixed VOCs, VOC diluted with nitrogen, or pure nitrogen) requires manually opening and closing the valves, as well as reconnecting the tubes.

Such manual operation introduces risks of disturbances like unstable flow rates and contamination from ambient air. Moreover, this setup requires continuous supervision, which makes long-term measure-

ments impractical. To overcome these limitations, the gas sensing setup is redesigned, which will be discussed in section 4.5.

3

Programme of Requirements

This chapter outlines the mandatory and trade-off requirements that need to be fulfilled during the design process. The mandatory requirements define the essential functionalities that the socket, chamber, and automated control system must achieve to ensure proper performance. In contrast, the trade-off requirements are desired features to increase user satisfaction.

Mandatory Requirements (MR)

MR.1 Socket Design

The socket design has some functional requirements that it shall meet.

- [MR.1.1] The socket shall be compatible with the QFN Package MLP5X5-24-OP-01 (24-lead, 5 mm × 5 mm MLP Open-cavity).
- [MR.1.2] The socket shall provide consistent and stable electrical contact between all 24 leads of the QFN-packaged PCS chip and the PCB through an anisotropic conductive sheet. An anisotropic conductive sheet is used to allow the package to be inserted and removed from the socket without the need for soldering.
- [MR.1.3] The socket material shall be heat-resistant and chemically resistant.
- [MR.1.4] The socket shall be removable from the PCB.
- [MR.1.5] The socket shall allow easy insertion and removal of the QFN-packaged PCS chip without damaging the exposed parts in the QFN package.

MR.2 Chamber Design

The chamber design has some functional requirements that it shall meet.

- [MR.2.1] The chamber shall form a closed environment around the chip to maintain a stable gas flow and prevent significant gas leakage into the surrounding area. A minor leakage is acceptable, provided it does not exceed a maximum of 0.1 ml/min.
- [MR.2.2] The chamber shall include a gas inlet and outlet that match the 1/16 inch outer diameter gas tubes to ensure a proper seal.
- [MR.2.3] The chamber shall be heat-resistant and chemically resistant.
- [MR.2.4] The chamber shall fit tightly to the socket to prevent gas leakage, but also allow frequent removal of the chamber from the socket.

MR.3 Automated Control System

The automated control system has some functional requirements that it shall meet. Figure 1.1 shows devices that are used in the gas sensing setup: the Bronkhorst mass flow controllers (MFC) and the RVM industrial microfluidic rotary valves. These devices are essential to regulate and direct the gas flow in the system.

-
- [MR.3.1]** The system shall communicate via serial ports with three Bronkhorst mass flow controllers and two RVM industrial microfluidic rotary valves.
 - [MR.3.2]** The system shall enable users to control the flow rate of three Bronkhorst mass flow controllers.
 - [MR.3.3]** The system shall enable users to control the position of two RVM industrial microfluidic rotary valves.
 - [MR.3.4]** The system shall display real-time data from all connected devices, enabling users to monitor flow rates and valve statuses.
 - [MR.3.5]** The system shall enable users to schedule flow rate, valve position, and concentration setpoints at specific times, and execute these profiles.
 - [MR.3.6]** The system should automatically check the validity of values entered by the user.
 - [MR.3.7]** The system should fill fields with valid default settings and should display valid user entry ranges.

Trade-Off Requirements (ToR)

ToR.1 Socket Design

- [ToR.1.1]** The socket should be screwless to reduce the chip replacement time.
- [ToR.1.2]** The socket should allow for manual disassembly from the PCB without soldering.

ToR.2 Chamber Design

- [ToR.2.1]** The volume of the chamber should be as small as possible to reduce the gas refresh time and maximize the gas concentration inside the chamber. In addition, the chamber must be suitable for use with short gas inlet and outlet tubes.

ToR.3 Automated Control System

- [ToR.3.1]** The COM ports of the devices should be saved for reuse in future sessions.
- [ToR.3.2]** The system should include predefined standard profiles for ease of use.
- [ToR.3.3]** The system should support saving new custom profiles.
- [ToR.3.4]** The user should be able to specify the path where the custom profiles are stored.
- [ToR.3.5]** The system should display the runtime information of the profiles, such as elapsed times, current steps, and target values.
- [ToR.3.6]** The system should display a setpoint graph of the selected concentration profile.

4

Design

This chapter describes the design process and provides the reasoning behind the choices made for the chamber, socket, and the automated control system, and how these choices align with the requirements described in chapter 3.

4.1. Shared Design Considerations Between the Socket and the Chamber

The chamber ensures a closed and stable environment around the QFN-packaged PCS chip, while the socket ensures consistent and stable electrical contact between the chip and the PCB. Together with the gas sensing setup, the sensing ink on the chip can interact with VOCs, leading to changes in the sensor readout, as explained in section 2.1. Since the chamber and socket are used in the same setup, they are exposed to the same thermal and chemical conditions. As a result, the chamber and the socket share several common design constraints and requirements.

4.1.1. Material Properties

In the gas sensing setup, different gases flow into the chamber at varying temperatures, exposing both the socket and the chamber to thermal variations. To prevent gas leakage or poor sensor readouts, the material of both components should not shrink due to heat exposure. Additionally, the components must also be chemically resistant to VOCs such as ethanol and acetone listed in section 2.2. These requirements are defined in [MR 1.3], [MR 2.3].

Two materials that meet these requirements are aluminium and polyetheretherketone (PEEK). The comparison was made between aluminium 6061 and INTAMSYS® PEEK, as these specific variants are readily available from the known suppliers and are suitable for computer numerical control (CNC) machining and Fused Deposition Modeling (FDM) 3D printing, respectively. Table 4.1 compares the relevant material properties of aluminium 6061 and INTAMSYS® PEEK. The values are based on data from [10] for aluminium 6061 and [11] for INTAMSYS® PEEK.

Table 4.1: Comparison of material properties: aluminium 6061 [10] vs INTAMSYS® PEEK [11]

Property	Aluminium 6061	INTAMSYS® PEEK
Tensile Strength (MPa)	260	99.9
Thermal Conductivity (W/m·K)	166	0.29
Melting Point (°C)	650	343

Aluminium 6061 offers significantly higher tensile strength and thermal conductivity than PEEK. This results in aluminium offering a higher resistance to mechanical failure and having more effective heat dissipation than PEEK. Furthermore, aluminium has a significantly higher melting point than PEEK, which is crucial for its deformability.

According to [12] and [13], aluminium and PEEK are both chemically resistant to several VOCs used in the gas sensing setup listed in section 2.2, including 2-nonanol, nonanal, tetradecane, 1-dodecanethiol, ethanol, 1-propanol, 2-propanol, methanol, acetone, α -pinene, α -terpinene, 1-butanol, toluene and 2-butanone (MEK).

These material properties make both aluminium and PEEK suitable concerning the durability, heat resistance, and chemical resistance, as required by the socket and chamber design requirements. However, aluminium should be reconsidered if corrosive gases are added to the list of target VOCs. For example, if ammonia is added, aluminium may become susceptible to degradation.

4.1.2. Production Constraints

To manufacture the designs in the desired material, several production constraints must be considered. A design from PEEK can be manufactured using FDM 3D printing, while a design from aluminium can be processed through CNC machining. However, both methods have limitations.

CNC machining offers high precision. However, it also has the following limitations:

- Internal rectangular shapes cannot be perfectly fabricated, since CNC tools only operate along linear and rotational paths. Therefore, the corners of the internal rectangle will always be rounded because of the radius of the CNC tool.
- Machining small components can be challenging because of the complexity of fixing the component during machining, which can affect precision.

FDM 3D printing has the following limitations:

- The minimum wall thickness is determined by the nozzle of the printer.
- Overhangs and steep angles require support structures, which can impact the print quality.
- Surfaces may become uneven or deformed during the removal of 3D printing support material.

4.1.3. Final Material Selection

Considering these material properties and production constraints, explained in subsection 4.1.1 and subsection 4.1.2, aluminium is the preferred material for the chamber and socket since it has better mechanical strength, heat dissipation, and thermal conductivity. Additionally, CNC machining is more precise than FDM 3D printing. However, because of the small, precise, and complex design, manufacturing the chamber and socket via CNC machining in aluminium will be challenging and expensive.

Due to budget constraints and the complexity of the design, PEEK was selected as the final material for both the chamber and the socket. It provides sufficient strength and chemical resistance and it is cheaper to produce using FDM 3D printing.

To reduce costs during the development phase, prototypes are first printed in Polyethylene Terephthalate Glycol (PETG) material using the Prusa MK3S 3D printer at the MakerLab located at the Science Center of TU Delft. These printers have a nozzle of 0.4 mm, which means that the minimum wall thickness for the design will be 0.4 mm.

4.2. Socket

To allow for easy insertion and replacement of the QFN-packaged PCS chip, a socket is used instead of soldering the chip directly into the PCB. This allows the QFN-packaged PCS chip to be replaced multiple times, which is necessary for testing various sensing inks printed on different chips. In addition, a stable electrical connection through an anisotropic conductive sheet must be ensured between the QFN-packaged PCS chip and the full PCB, which is designed by the PCB subgroup [14]. The socket and the chamber are able to create a closed environment to maintain a stable gas concentration inside the chamber. Lastly, the socket must provide physical protection for the QFN-packaged PCS chip against environmental damage, such as accidental drops during the experiment. The detailed dimensions of the socket can be found in Appendix A.2.

As shown in Figure 4.1, a square hole is designed in the center to place the QFN-packaged PCS chip. Additionally, two opposing tweezers holes are designed to allow easy insertion and removal of the QFN-packaged PCS chip.

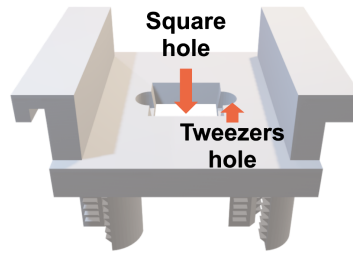


Figure 4.1: 3D rendering of the socket from a top view

4.2.1. Socket-PCB Connection

The purpose of the socket-PCB connection is to provide a strong mechanical connection and a stable electrical connection between the socket and the PCB. To meet the trade-off requirement [TOR.1.1] and [TOR.1.2], the socket-PCB connection should eliminate screws, while remaining removable by hand. Various design considerations were evaluated, as shown in Appendix B, with focus on minimizing material usage, reducing PCB deformation, and maximizing user satisfaction. Table 4.2 summarizes the advantages and disadvantages of these designs. For a more detailed discussion, see Appendix B.

Table 4.2: Comparison of socket-PCB connection mechanisms

Mechanism	Advantages	Disadvantages
Usage of rubber	- Provides a strong mechanical hold	- Difficult to remove - Hard to find in the exact size and shape that fits the socket - Potential wear and tear over time
Press-fit Single use	- Provides a strong mechanical hold	- Single use only - May damage PCB during removal - Requires high precision in design
Press-fit Cap	- Compact and low-complexity design - Easy to disassemble and assemble	- Requires high precision - Weak mechanical hold - Potential wear and tear over time
Snap Ring	- Compact and low-complexity design - Easy to disassemble and assemble	- Weak mechanical hold - Potential wear and tear over time
Barbed Rivets	- Provides strong mechanical hold - Compact and low-cost - Easy to disassemble and assemble by hand	- Potential wear and tear over time

Based on the comparison of advantages and disadvantages, the final connection design utilizes barbed rivets. Figure 4.2 shows a 3D rendering of the socket and Figure 4.3 shows a 3D rendering of a single barbed rivet. Each barbed rivet has 4 lateral sides and each side has 7 barbs with an angle of 45 degrees. The total number of barbs was chosen to match the rivet length, aiming to ensure a stable attachment of the socket to the PCB.

This design replaces the need for screws [TOR.1.1] and allows the socket to be disassembled from the PCB by hand [TOR.1.2]. The latter requirement is verified through manual disassembled trials conducted during prototyping. Although the socket is designed to be removed by hand, the use of a tool

such as pliers is recommended in practice to avoid transferring contaminants from gloves to the socket. The technical drawings of the socket and a single barbed rivet are provided in section A.2.

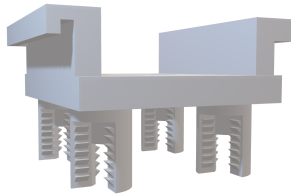


Figure 4.2: 3D rendering of the socket from a front view

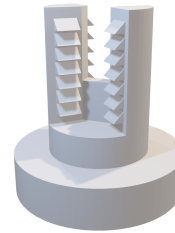


Figure 4.3: 3D rendering of the barbed rivet

4.2.2. Anisotropic Conductive Sheet

To ensure the electrical connection between a chip and a PCB, typically, conventional pogo pins or metal spring contacts are used. More recently, anisotropic conductive films (ACFs), adhesive (ACAs) and sheets (ACSs) are increasingly applied for chip interconnection because they provide high resolution, lightweight, thin profile, and low power consumption [15]. These properties make them suitable for compact electronic systems.

In this design, an anisotropic conductive sheet from the ShinEtsu MT-type series is placed between the socket and the full PCB. This enables stable vertical (z-axis) electrical interconnection, while still allowing for quick and easy replacement of the QFN-packaged PCS chip [16]. This sheet has a thickness of 0.5 mm and an approximate lateral offset of 0.25 mm, which must be taken into account on all four sides of the 5 mm x 5 mm QFN package to ensure electrical contact. Figure 4.4 illustrates the placement of the offset. Figure 4.5 shows the intended place for the ACS, indicated by a red arrow pointing to a square-shaped indent on the bottom side of the socket. This indent is designed with the offset already accounted for, which helps ensure accurate positioning of the ACS.

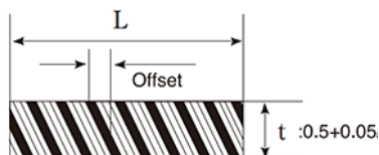


Figure 4.4: Cross-sectional view of the anisotropic conductive sheet [16]

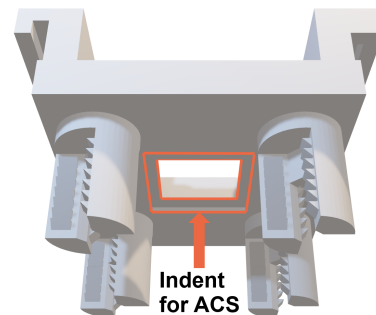


Figure 4.5: 3D rendering of the socket from a bottom view

4.3. Adapter PCB

An adapter PCB was designed to validate the socket configuration independently of the full PCB. Its primary purpose is to ensure a stable electrical connection between the QFN-packaged PCS chip and the anisotropic conductive sheet. For testing purposes, the sensor board from the previous e-nose system has been reused. This board includes a 224-1275-00-0602J connector socket, which is used to connect to the designed socket. However, since the contacts of the connector socket align with the position of the barbed rivets of the designed socket, it is not possible to place the pin headers in the same position. To resolve this issue, an intermediate adapter PCB is introduced. A visualization of the adapter PCB setup is shown in Figure F.1. Although the intermediate adapter PCB may cause some parasitic effects, such as increased resistance, it is acceptable for the primary purpose, which is to ensure a good electrical connection between the QFN-packaged PCS chip and the anisotropic conductive sheet.

4.3.1. Adapter PCB Layout

The layout of the adapter PCB is shown in Figure 4.6. The QFN package footprint is located in the center and the four blue circles represent the footprints of the holes used for the barbed rivets of the designed socket. These barbed rivets are inserted through these holes, securing the socket in place. The required lateral offset of the anisotropic conductive sheet, as discussed in subsection 4.2.2, has also been taken into account in the layout of the adapter PCB by shifting the position of the QFN package footprint by 0.25 mm to the right. The board was designed using KiCad, an open-source PCB design tool.

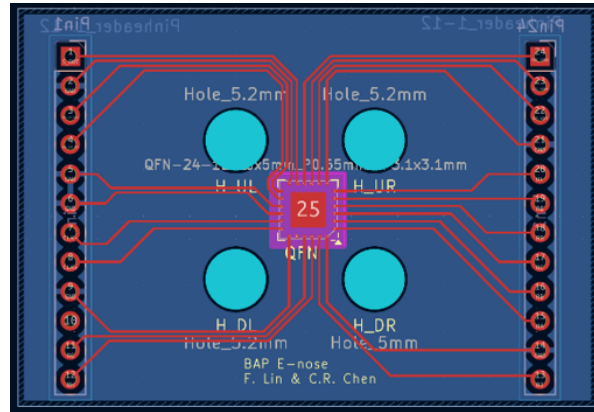


Figure 4.6: Wiring diagram of the adapter PCB

To ensure compatibility with the sensor board of the previous e-nose system, the pinout of the currently used QFN package was remapped to match that of the previous CDIL24 package. In Figure 4.7, the QFN package is shown on the left and the previous CDIL24 package on the right. This remapping ensures that all signals are routed to the connector pins expected by the sensor board. For example, pin 5 of the QFN package is routed to pin 1 of the pin header for the connector socket, because its position originally carried the S_OUT signal in the CDIL24-based design.

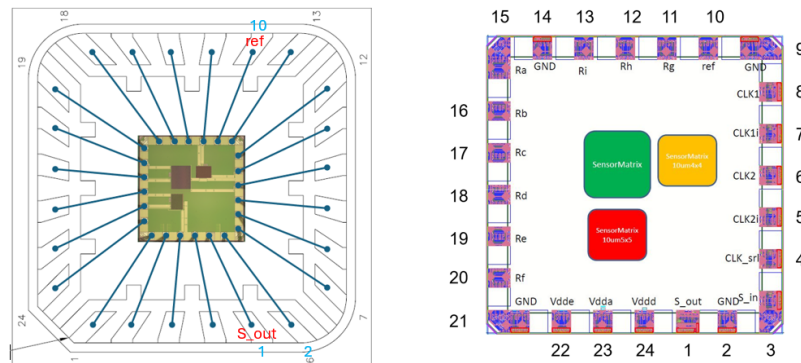


Figure 4.7: QFN24 package to CDIL24 package mapping

Several constraints were taken into account during the layout design. One of the considerations was the routing of the differential clock traces (CLK+ and CLK-). Ideally, these traces should be as short as possible. However, the placement of the four holes for the socket limited the flexibility of routing. To maintain signal integrity, CLK+ and CLK- were intentionally routed closely in parallel and matched in length. This layout helps the magnetic fields generated by the two signals cancel each other out, thereby reducing electromagnetic interference (EMI). In addition, they were also routed as far as possible from other signal traces to minimize coupling. This is because capacitive and inductive coupling between two unrelated nearby parallel traces can cause crosstalk and degrade signal quality as described by Texas Instruments [17]. In addition, all readout traces are approximately matched in length

to maintain signal timing. Finally, pin 10 of the CDIL24 package, which corresponds to the 'ref' signal, should be interrupted on the adapter PCB, as it is not used.

4.4. Chamber

The chamber should ensure that gas from the gas sensing setup is exposed to the sensing ink on the QFN-packaged PCS chip while preventing leakage into the surrounding area. To meet the mandatory requirements and trade-off requirements for the chamber design as described in chapter 3, several key design considerations were addressed. Based on these considerations, the final chamber was designed with a total volume of 24.75 mm³. The detailed dimensions of the chamber can be found in Appendix A.3.

4.4.1. Gas In- and Outlet

Gas flows into the chamber through an inlet and outlet tube. These tubes are inserted directly into the chamber to ensure that the gas reaches the QFN-packaged PCS chip. For this purpose, a PTFE tube with an inner diameter of 1/32 inch and an outer diameter of 1/16 inch is used.

The positioning of the inlet and outlet has a significant role in measuring the accurate gas sensor responses. A study by F. Annanouch et al. [18] concluded that a boat-shaped design with tangential gas flow ensures a more homogeneous gas distribution, leading to faster, more stable, and stronger sensor responses than a cross-shaped design with perpendicular gas flow, as shown in Figure 4.8. Based on these findings, the chamber was designed following a boat-shaped configuration with tangential gas flow. Furthermore, placing the gas inlet and outlet tubes directly opposite each other, as in the cross chamber, the gas may exit the chamber before it has sufficiently contacted the chip sensing surface. This reduces the effective exposure time and makes the detection of VOCs more difficult.

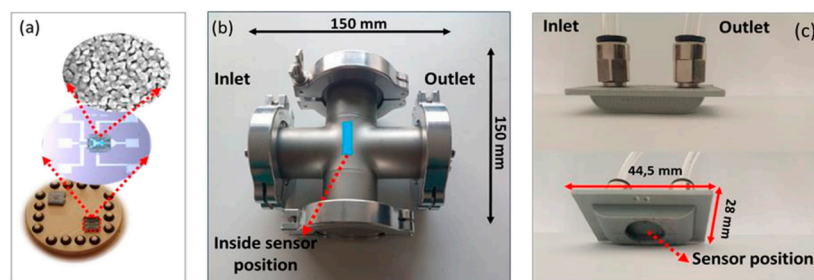


Figure 4.8: Photographs of: (a) SnO₂ Sensor; (b) Cross Chamber; (c) Boat Chamber [18]

To implement a boat-shaped chamber with tangential gas flow, two holes are designed on the top of the chamber for the gas inlet and outlet tubes. To determine the optimal size for the gas tube, a fit test was conducted by prototyping a test plate with multiple hole diameters. This iterative process showed that a 2.00 mm diameter hole allows the gas tube to fit firmly into the chamber.

To ensure that the tubes remain in place, each hole begins with a 3.00 mm deep vertical cylindrical section with a diameter of 2.00 mm. To prevent the tube from being inserted too far into the chamber, the final 3.00 mm of this hole is tapered from a cylindrical section of 2.00 mm diameter to 1.39 mm diameter, as shown in Figure 4.9. This ensures that the tube can be easily inserted while providing a mechanical stop that prevents over-insertion, fulfilling [MR.2.2] of chapter 3, which requires the gas inlet and outlet to match the gas tube dimensions to ensure a proper seal.

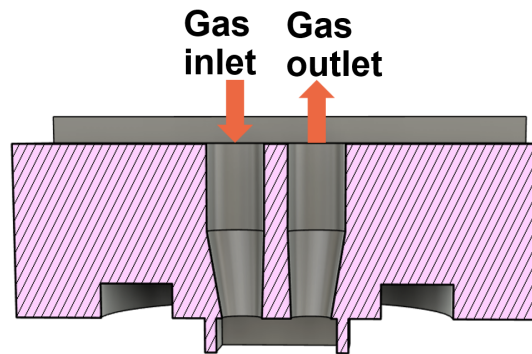


Figure 4.9: Cross-sectional view of the gas chamber inlet and outlet hole

4.4.2. Chamber Socket Connection

The chamber must form a closed environment around the QFN-packaged PCS chip to maintain a stable gas flow and prevent gas leakage into the surrounding area. To achieve this, the chamber should firmly connect to the socket that holds the chip. This connection should ensure no gas leakage into the surrounding area during operation.

Different designs were considered for the chamber-socket connection. The advantages and disadvantages of these designs are evaluated and compared in Table 4.3. For an extended explanation of these mechanisms, see Appendix C.

Table 4.3: Comparison of chamber-socket connection mechanisms

Mechanism	Advantages	Disadvantages
Clamshell spring socket	- Provides a strong mechanical hold	- Increases mechanical complexity due to parts like springs or levers, which may reduce reliability and stability
Socket-PCB-Based fixation	- A single connection that locks the chamber, socket, and PCB together - Ensures good alignment and pressure	- Removal requires full disassembly from PCB - Not user-friendly for frequent assembly and disassembly
C-shaped slider	- Compact and low-complexity design - Easy to disassemble and assemble	- Potential wear and tear over time

After comparing mechanical complexity and user friendliness, the C-shaped slider, shown in Figure 4.10, was selected as the final design. Detailed dimensions of the C-shaped slider are provided in Appendix A.4. The C-shaped slider design was inspired by the zip-lock bag, which operates similarly to a zip fastener. These mechanisms are known for enabling simple and repeatable opening and closing operations. This approach supports [MR.2.4] of chapter 3, which requires the chamber-socket connection to be suitable for frequent removal.

To allow integration of the slider, the chamber and the socket include slight extensions on both sides along one axis. These extensions of the protruding parts have an indentation that matches the slider's shape, as shown in Figure 4.10. This ensures that the slider can smoothly move over the indentations in the protruded part, which results in a mechanical connection that is both robust and repeatable.

To ensure that the sliders are mechanically locked, the indentations in the protruded part of the chamber and the socket are closed at one end. This design allows the slider to be inserted from only one direction, increasing the safety of the connection.

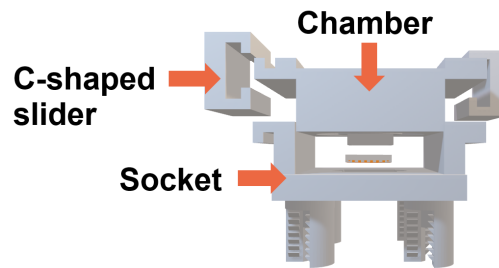


Figure 4.10: 3D rendering of the chamber and socket with the C-shaped slider

4.4.3. Square Support Frame

To fulfill [ToR.2.1] of chapter 3, which states that the volume of the chamber should be minimized to reduce the gas refresh time and maximize the gas concentration, the chamber should exactly match the size of the QFN package (5 mm × 5 mm). At the same time, to meet [MR.1.2], which requires that the socket can provide electrical contact between the QFN-packaged PCS chip and the PCB through an anisotropic conductive sheet, the QFN-packaged PCS chip must be pressed. This is achieved by designing a chamber that presses against the black edges of the QFN package (shown in Figure 4.11). For this purpose, a square support frame was designed, as shown in Figure 4.12. The dimensions of the QFN package are shown in Appendix A.1.

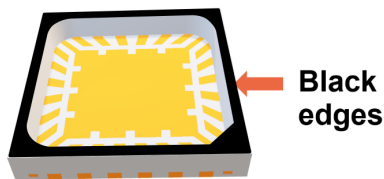


Figure 4.11: 3D rendering of the QFN MLP5X5-24-OP-01 package [9]

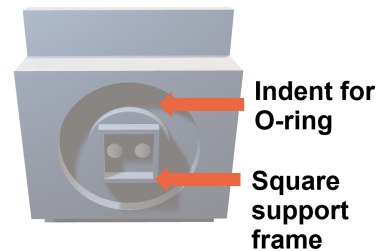


Figure 4.12: 3D rendering of the chamber highlighting the O-ring indent and the square support frame

Due to the limitations of the 3D printer, which has a 0.4 mm nozzle, it is not feasible to print a wall that matches the 0.125 mm wide black edges, as explained in subsection 4.1.2. As a result, the wall thickness of the square support frame was set to 0.4 mm. However, this slight increase is not expected to cause issues, as the black edges of the QFN package have a height of 0.597 mm and the chip lies below this level. Therefore, the support frame will not come into contact with the PCS chip.

When the support material is removed, the surfaces can be uneven or deformed. To compensate for this, an O-ring is placed around the square support frame. O-rings are commonly used to seal different parts and prevent leakage of fluids and gases. In this design, an indentation for an O-ring is included to hold the O-ring and to allow it to protrude slightly above the square support frame. This ensures that, when the socket and chamber are fastened using the C-shaped slider, the O-ring is compressed and compensates for the surface irregularities to form a reliable seal. Polydimethylsiloxane (PDMS) O-rings have been used in the design because they have a low Shore hardness, which allows them to deform easily and adapt to uneven surfaces.

4.5. Automated Control System

To address the limitations in the previous gas concentration system setup, as discussed in section 2.2, the gas sensing setup has been redesigned. This new setup consists of three Bronkhorst mass flow controllers (MFCs), two Torrey Pines IC20XR digital chilling/heating dry baths, and two RVM industrial microfluidic rotary valves, shown in Figure 4.13. These devices allow for precise and programmable control of gas mixing. This also enables the implementation of an automated control system that improves efficiency and reduces operational time.

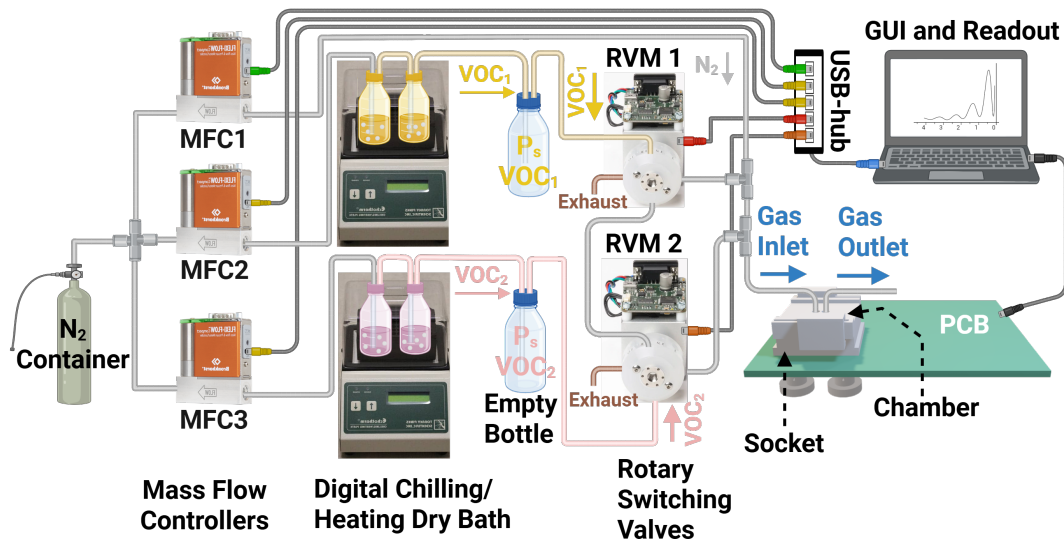


Figure 4.13: Gas sensing setup for testing pure and mixing two VOCs

The setup displayed in Figure 4.13 operates as follows. Three Bronkhorst mass flow controllers (MFCs) are connected to a nitrogen gas container. Each MFC individually regulates the flow rate for a separate gas path: one delivers pure nitrogen for dilution, while the other two guide nitrogen through separate bottles containing different VOCs (VOC1 and VOC2). These bottles are placed on the digital chilling/heating dry bath to maintain constant temperature, ensuring a stable vapor pressure and preventing condensation.

Nitrogen gas is introduced into the bottles with a VOC liquid, generating bubbles as it flows through the VOC. These bubbles contain nitrogen and VOC, which float to the surface of the VOC liquid. Upon reaching the surface, the bubbles burst, releasing a gas containing nitrogen and VOC. The resulting VOC nitrogen streams are then directed into an empty bottle to equalize the pressure with the atmosphere.

All three gas streams (VOC1, VOC2 and pure nitrogen) are directed to two 4-port rotary switching valves, which operate together to control the gas composition directed to the chamber (pure nitrogen, VOC1 diluted with nitrogen, VOC2 diluted with nitrogen or VOC1 mixed with VOC2). After the valves switch to the desired configuration (which will be explained in subsection 4.5.3), the selected gases are mixed through a T-connector and directed to the chamber through a tube. This tube should be kept as short as possible, as a shorter length reduces the impact of Taylor dispersion, leading to less axial spreading of the gas. Additionally, a shorter tube leads to faster replacement of the previous gas. A more detailed explanation of Taylor dispersion can be found in Appendix D.2.

Once inside the chamber, the gas interacts with the sensing ink on the QFN-packaged PCS chip. This interaction causes a change in capacitance as explained in section 2.1. By comparing the capacitance before and after VOC exposure, the system can detect the presence of VOCs. This information can be obtained using an existing readout application developed in MATLAB.

4.5.1. Bronkhorst Mass Flow Controller - FLEXI-FLOW

The Bronkhorst mass flow controller (MFC) with the model Flexi-Flow is selected because of their compact size (60 mm x 20 mm), accuracy up to $\pm 0.5\%$ of the reading (Rd) plus $\pm 0.1\%$ of the full scale (FS), with FS defined as 5 ml/min, and fast response time (settling time <150 ms) according to the datasheet [19]. Unlike the syringe pumps used in the previous setup, MFCs allow continuous gas flow without the need for refilling nitrogen in the syringes. Most importantly, they can be fully controlled

via the Bronkhorst Python package. This replaces the manual setting of flow rates with buttons on the syringe pumps required in the older configuration.

4.5.2. The Digital Chilling/Heating Dry Bath

The digital chilling/heating dry bath provides temperature control ranging from $-10\text{ }^{\circ}\text{C}$ to $110\text{ }^{\circ}\text{C}$, with an accuracy of $\pm 1\text{ }^{\circ}\text{C}$ [20]. Unlike the ice bath used in the previous setup, this device can maintain a stable temperature without manual adjustment. Moreover, this device does not need to be actively controlled by the automated control system, because the desired temperature is fixed in advance.

The main purpose of temperature control is to prevent gas diffusion and condensation. To avoid condensation, the temperature of the VOC nitrogen stream should be lower than the ambient temperature of the chamber. However, according to the device specifications, the dry bath can lower the temperature by up to $30\text{ }^{\circ}\text{C}$ below the ambient temperature [20]. The flat aluminium plate of the dry bath provides direct thermal contact with the VOC bottles. In addition, the bottles are placed inside a metal grid holder that ensures efficient thermal conduction. Therefore, it is reasonable to assume that the temperature of the VOC gas closely matches the plate temperature. The target temperature is set to $0\text{ }^{\circ}\text{C}$ to prevent condensation of the VOC nitrogen stream upon entering the sensing chamber. At this temperature, condensation is unlikely, as VOCs are already evaporated at room temperature. As mentioned, the system can reduce the VOC temperature by up to $30\text{ }^{\circ}\text{C}$ below the ambient temperature. Since the typical laboratory temperatures range between $20\text{ }^{\circ}\text{C}$ and $25\text{ }^{\circ}\text{C}$, a target temperature of $0\text{ }^{\circ}\text{C}$ is therefore feasible.

4.5.3. RVM Industrial Microfluidic Rotary Valve - FAST Model

The RVM industrial microfluidic rotary valve is selected for its compact design, fast port-to-port-switching ($< 136\text{ ms}$) and chemically resistant wetted materials (PCTFE and PTFE) [21]. It supports various port configurations and can be controlled via USB or serial communication interfaces, such as RS232 and I2C. Furthermore, its tube-like fluidic path minimizes dead volume, which reduces cross-contamination between measurements. Dead volume refers to a part of the internal volume where little or no flow occurs. A minimized dead volume is particularly important in the gas sensing setup, as accurate detection of various VOCs depends on it. Lower cross-contamination between measurements leads to more reliable results.

Unlike the manually operated shut-off valves used in the previous setup, this valve allows for automated switching between gas flow paths. As shown in Figure 4.14, each valve has two positions, with each position corresponding to a distinct flow path.

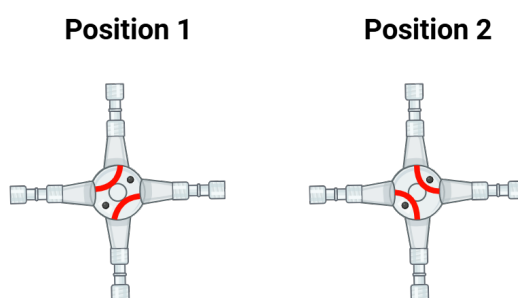


Figure 4.14: Valve positions

The gas sensing setup contains two valves, as illustrated in Figure 4.13. By switching the valves between different positions, different gases can be routed into the chamber via the gas inlet. The valve located at the top of Figure 4.13 is referred to as valve 1, while the one at the bottom is referred to as valve 2. The gas stream directed into the chamber depends on the combination of the valve positions, as summarized in Table 4.4.

Table 4.4: Valve configuration and resulting gas stream

Gas Stream to Chamber	Valve VOC 1	Valve VOC 2
VOC 1 diluted with nitrogen	Position 2	Position 2
VOC 2 diluted with nitrogen	Position 1	Position 1
VOC 1 and VOC 2 mixed	Position 2	Position 1
Pure nitrogen	Position 1	Position 2

4.5.4. Graphical User Interface

To allow users to monitor and control the gas sensing setup, a graphical user interface (GUI) has been designed as part of the automated control system with Python. The interface has been implemented using the Tkinter library.

The GUI should allow the user to connect and disconnect the mass flow controllers and rotary valves. It should also provide options to configure COM ports and directory paths to save profiles. In addition, users must be able to manually control MFCs and valves, as well as create, execute, and monitor time-based profiles. It should also provide real-time feedback, including device connection status, current flow rates, and valve positions, offering a clear overview of the system's state. Each tab within the GUI has its own functionality:

- Device Control Tab: Enables manual control of flow rates and valve positions, while displaying real-time data from these devices.
- Profile Management Tabs: Enable users to create, save, load, edit, and execute custom time-dependent profiles. Users can schedule flow rate, valve position, and concentration setpoints at specific times, and execute these profiles, such that [MR.3.5] is met.

The following profile types are supported:

- MFC profile management: Time-based control of the flow rates.
 - Valve profile management: Time-based control of the valve positions.
 - MFC and valve profile management: Time-based control of flow rates and valve positions.
 - Pure gas ON/OFF profile management: Allows users to define and run profiles that alternate between VOC and nitrogen flow, based on the selected VOC type, target concentration, and ON/OFF durations. During the ON phase, VOC is diluted with nitrogen and flows into the chamber over the QFN-packaged PCS chip, while during the OFF phase, only pure nitrogen flows is delivered.
 - Pure gas different concentration profile management: VOC concentration is controlled over time based on the selected type and target concentration at each time step to produce the desired gas mixture.
- Multiple Profile Runner: A panel that allows users to select and execute one MFC profile and one valve profile simultaneously.

While a profile is running, the GUI should display real-time information, including the elapsed time, the current step, and other relevant variables. This also allows users to track progress. To keep the user interface responsive during long-running executions of the profile, threading is used. This ensures that device commands are executed without blocking the main GUI thread. For error-handling, Python's try/except blocks are implemented throughout the code to catch unexpected errors, such as input errors and connection failures. The error will be provided to the user via message boxes.

To support calibration and testing with different or repeat the same concentration of the gases (VOC 1, VOC 2, or pure nitrogen), the GUI should display a setpoint concentration graph in the pure gas ON/OFF profile management and pure gas different concentration profile management. This graph represents the target VOC concentration over time and serves as a reference to verify whether the sensor output follows the expected pattern based on the concentration setpoints. This is because the sensing ink on the QFN-packaged PCS chip interacts with the VOC, leading to a change in capacitance as explained in section 2.1. Higher VOC concentrations lead to larger changes in capacitance.

As a result, the sensor output changes in response to the concentration of the introduced gas into the chamber. When the valves switch the gas stream to the chamber from nitrogen to a VOC, for example, a noticeable shift in the readout signal is expected. By comparing this signal to the predefined setpoint graph, it can be determined which sensor output corresponds to which VOC concentration. This is important for interpreting the measurements and to calibrate the system.

Once the user selects either a pure gas ON/OFF profile management or a pure gas different concentration profile, and specifies the concentration of the VOC and durations, the system should automatically adjust the MFC flow rates to achieve the corresponding VOC concentration. This calculation is based on the Antoine equation [22] and Dalton's Law of Partial Pressures [23], to determine the correct flow rates for the desired VOC concentration in parts per million (ppm). The final expression, derived in section E.1, is shown below as Equation 4.1:

$$f_{VOC} = C(f_{VOC} + F_{N_2}) \frac{P}{P_{\infty} e^{-\frac{T_B}{T+T_C}}} = C f_{total} \frac{P}{P_{\infty} e^{-\frac{T_B}{T+T_C}}} \quad (4.1)$$

where

- f_{VOC} is the flow rate of the VOC-enriched nitrogen stream in ml/min
- C is the concentration of the VOC
- F_{N_2} is the flow rate of pure nitrogen gas as a dilution in ml/min
- f_{total} is the total flow rate in ml/min which is equal to $f_{VOC} + F_{N_2}$
- P_{∞} is 10^A , with A being the Antoine coefficient A
- T_B is $B \ln(10)$ in $^{\circ}\text{C}$, with B being the Antoine coefficient B
- T_C is the Antoine coefficient C in $^{\circ}\text{C}$
- T is the temperature of the VOC in $^{\circ}\text{C}$
- P is the atmospheric pressure of 760 mmHg

It is important to note that the Antoine equation only holds in thermal equilibrium. Before starting each experiment, it is crucial to set the temperature of the VOCs to a stable temperature. In this setup, the digital chilling/heating dry bath is used to manually set the VOC temperature to 0°C before each experiment. This is to ensure a stable vapor pressure and avoid condensation inside the chamber. Furthermore, the Antoine equation uses Antoine coefficients that are specific to a particular VOC and are only valid within a certain temperature range. The Antoine coefficients used in the system are listed in Appendix E.1. In practice, the actual VOC concentrations may deviate from the calculated values due to various limitations:

- Inaccuracies of mass flow controllers: Each mass flow controller has an accuracy up to $\pm 0.5\%$ of the reading (Rd) plus $\pm 0.1\%$ of the full scale (FS), with the full scale defined as 5 ml/min.
- Inaccuracies of the digital chilling/heating dry bath: The digital chilling/heating dry bath has an accuracy up to $\pm 1^{\circ}\text{C}$, which directly influences vapor pressure.
- Tube length effects: The use of PTFE tubing, although chemically resistant, introduces two potential sources leading to inaccuracies. First, the PTFE tube has low thermal conductivity [24], but this may lead to temperature loss along the path when the tube is long, which could affect the vapor pressure and therefore the concentration. Second, longer tubes increase the higher flow resistance, which can influence the effective flow rate. These effects are minimized by keeping the tubing as short and straight as possible.

As a result, a margin of error of 10% in VOC concentration is considered acceptable for this setup, assuming minimal tubing length. This margin is supported by a worst-case analysis, the details of which are documented in Appendix E.2.

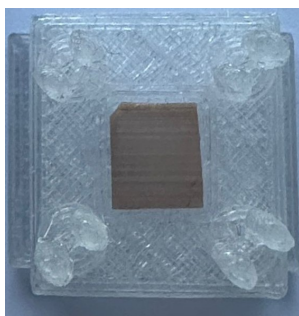
5

Results

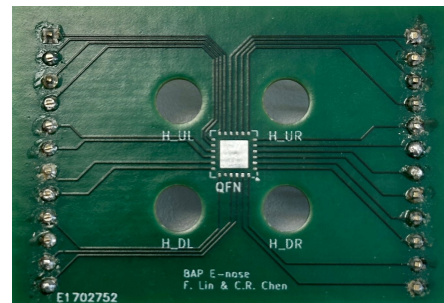
This chapter discusses the prototype implementation, the used testing setup, and the validation of the results.

5.1. Socket

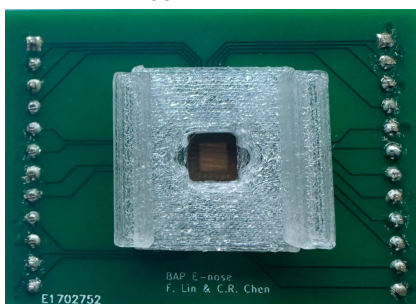
Figure 5.1 shows the assembly of the QFN-packaged PCS chip, the anisotropic conductive sheet, the socket, and the adapter PCB. The electrical connection through ACS was verified using a multimeter in continuity mode. In this mode, the multimeter applies a small current between two contact points and checks whether a continuous low-resistance electrical path exists between them. One of the test probes was placed on a pad of the QFN package, while the other was placed on the corresponding pin header of the adapter PCB. A successful continuity reading confirmed a functional electrical connection between the QFN-packaged PCS chip and the adapter PCB.



(a) Bottom view of socket with the ACS



(b) The adapter PCB



(c) Socket with ACS in the adapter PCB



(d) QFN-packaged PCS chip in the socket

Figure 5.1: Assembly of the QFN-packaged PCS chip, the ACS, the socket and the adapter PCB

5.2. Chamber

To validate that the chamber-socket connection is gas-tight, the experimental setup shown in Figure 5.2 was used. The actual setup is illustrated in Appendix G.2.

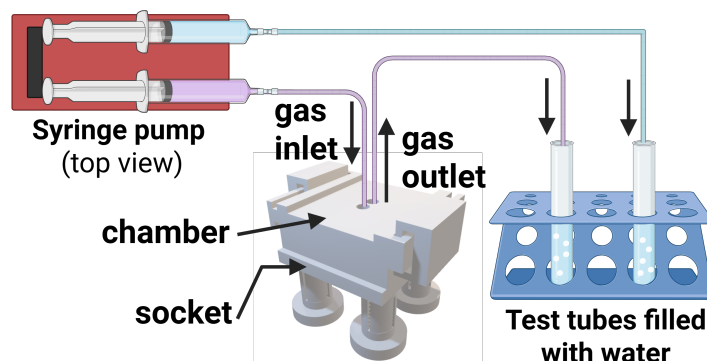


Figure 5.2: Schematic of the chamber leakage experimental setup

Two syringes were placed on the syringe pump, each connected to a separate test tube filled with water. One syringe was connected directly to its test tube and served as a reference. The other syringe pushed air through the inlet of the chamber, allowing it to pass through the chamber and exit via the outlet into the second test tube. If both test tubes produced the same number of bubbles over a fixed period of time, then it can be concluded that there was no gas leakage in the chamber.

This test was repeated five times, with all results within the acceptable margin of error of 0.1 ml/min. The maximum deviation observed in the test is five bubbles per minute, shown in Table 5.1. Assuming that a bubble has a diameter of 3.00 mm, which corresponds to a volume of $1.413 \cdot 10^{-8} \text{ m}^3$, the maximum estimated chamber leakage was approximately 0.07 ml/min. This confirms that full chamber–chip–socket assembly, held in place by the C-shaped sliders, provides sufficient sealing for the gas flows used in the gas sensing setup, where the maximum allowable leakage was defined as 0.1 ml/min.

Table 5.1: Number of bubbles observed in 1 minute at different flow rates for direct vs via the chamber

Flow Rate (ml/min)	Number of Bubbles in Test Tube 1 (Direct)	Number of Bubbles in Test Tube 2 (Via the Chamber)
0.3	21	18
0.5	35	31
0.7	51	46
1.0	68	66
1.2	83	81

5.3. Automated Control System

5.3.1. Valve Position Setup

To validate the valve position and the internal connection of the valve, the experimental setup shown in Figure 5.3 is used. Two syringes were placed on the syringe pump and connected to the valve's inlet ports. Tubes connected to the outlet ports were placed into test tubes filled with water.

By activating only one syringe at a time and switching between valve positions 1 and 2, the flow path, and thus the internal connection, was identified by observing in which test tube bubbles appeared at each valve position. The schematic setup and valve flow paths are shown in Figure 5.3.

The same test was repeated using the LSPOneQuick application provided by the manufacturer. The outcome confirmed that the observed internal connections matched those specified by the manufacturer. The actual setup is illustrated in Appendix G.1.

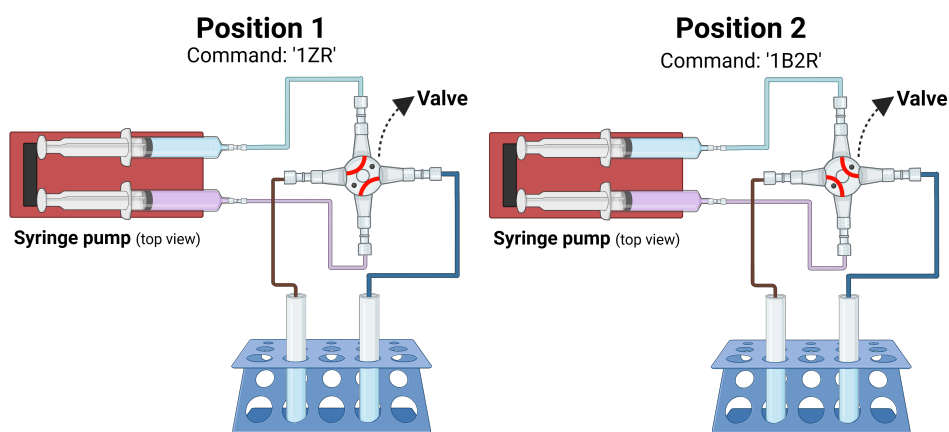


Figure 5.3: Schematic of valve connection and position validation

5.3.2. Graphical User Interface

As described in subsection 4.5.4, the GUI is organized into several tabs. These tabs are scrollable to ensure usability of the GUI regardless of screen size.

The header of the GUI remains visible regardless of the user's active tab. It displays the COM-port and the connection status of each device, as shown in Figure 5.4.

The header also includes a button to open the connection settings tab, where users can change and save the COM-port of each device, and specify the directory path to store the profile data, displayed in Figure 5.5. These settings are saved in JSON format, which allows the saved data to be easily reloaded.

Another button in the header is to navigate to VOC manager, which allows the user to add, edit, or delete VOC entries, shown in Figure 5.6. Users can add desired VOCs by entering the VOC name, Antoine coefficients (A, B, and C) and valid temperature range for those coefficients. The VOC list can be edited, saved, and deleted when required.



Figure 5.4: Device connections

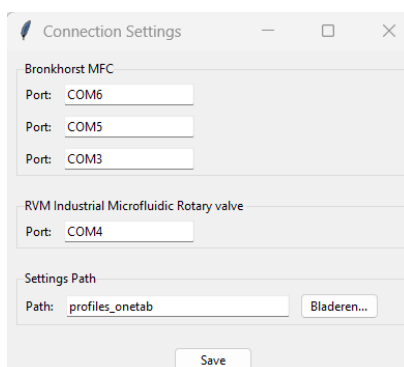


Figure 5.5: Connection settings

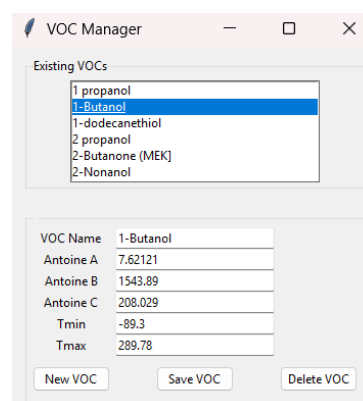


Figure 5.6: VOC Manager

Additionally, the status bar in the header provides system events and real-time readings, as shown in Figure 5.7.

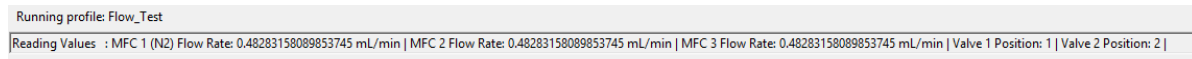


Figure 5.7: Status bar

The header also includes a live profile panel that displays an overview of all profiles during execution, showing the elapsed time, current step, and the currently set values, visualized in Figure 5.8. This overview is updated through a callback mechanism, in which a function is passed as an argument to another function. During the execution of the profile, the function to run the profile is called at each step with the current profile data, allowing the profile overview to be updated and visualized in the GUI.

Profile	Elapsed Time	Step	Value
MFC Running Profile	-	-	-
Valve Running Profile	-	-	-
MFC and Valve Running Profile	2.0s	1/7	MFC 1: 0.50 ml/min, MFC 2: 0.50 ml/min, MFC 3: 0.50 ml/min, Valve 1: Position 1, Valve 2: Position 2
Pure Gas Different Concentration Running Profile	-	-	-

Figure 5.8: Profile overview

Furthermore, the system automatically validates the user inputs and displays error messages when invalid inputs are entered by the users, such as non-numeric concentration or a negative flow rate, as illustrated in Figure 5.9 and Figure 5.10.

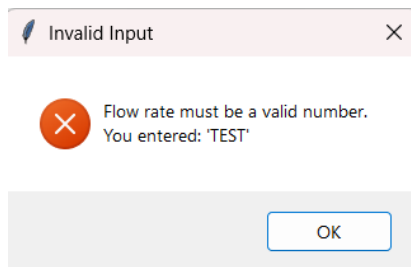


Figure 5.9: Invalid flow rate input

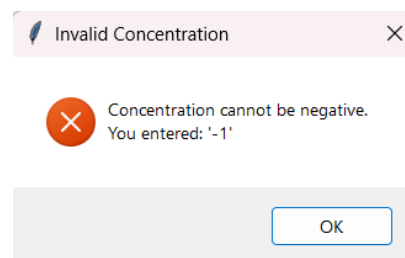


Figure 5.10: Invalid concentration input

During startup or when creating a new profile, the system also automatically fills input fields with default settings retrieved from an initialization file. Valid input ranges for the flow rate, valve positions, and concentration are displayed in each tab. The range for the flow rate and valve positions can be modified via the init file. The range for the VOC concentration is calculated using Equation E.5, based on the selected VOC type.

Device Control

Within the device control tab, users can manually control the MFCs and the rotary valve, as shown in Figure 5.11. Each device can be connected and disconnected. This tab also displays the target and the real-time readings from each device.

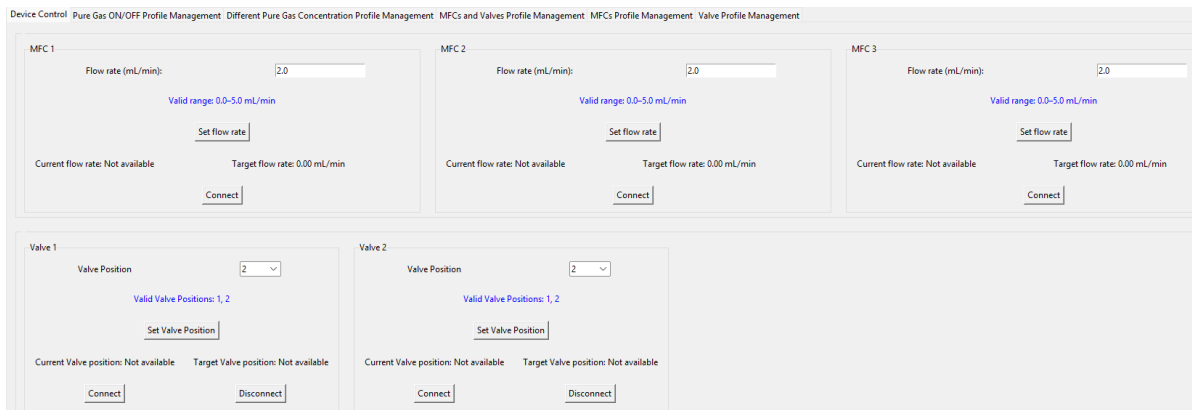


Figure 5.11: Device control tab

Several profile management tabs are implemented to allow users to create, load, edit and execute those time-dependent profiles.

Pure Gas ON/OFF Profile Management

The pure gas ON/OFF profile management, shown in Figure 5.12 is used to obtain the calibration for the sensor output by exposing the QFN-packaged PCS chip with a flow of VOC diluted with nitrogen in an ON/OFF pattern. The user selects the MFC connected to the VOC, specifies the VOC type, target concentration (ppm), and total flow rate.

By clicking the "Calculate Flow" button, the required VOC and nitrogen flow rates are computed using Equation E.6 and the Antoine coefficients stored in the VOC manager.

The user also needs to specify the ON and OFF time. During the ON phase, VOC is diluted with nitrogen and flows into the chamber, while during the OFF phase pure nitrogen flows into the chamber. The positions of the valves are automatically set based on the selected MFC associated with the VOC and the current ON/OFF phase, following the configuration in Table 4.4. The ON/OFF graph shows the valve switching behavior and the applied VOC concentration during the ON cycle, which can be used to calibrate the sensor output.

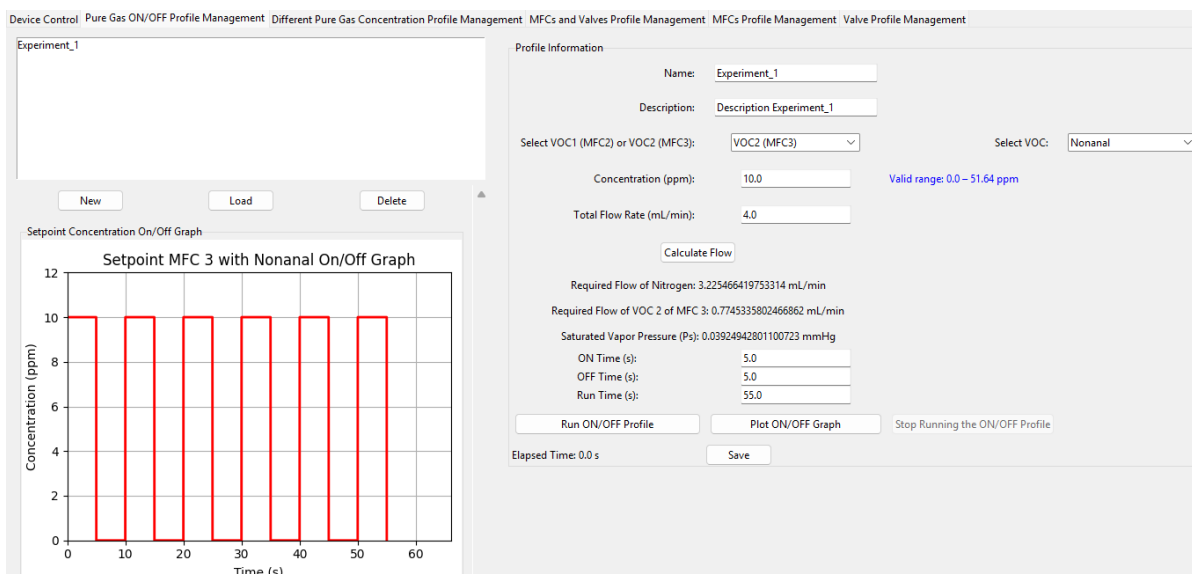


Figure 5.12: Pure gas ON/OFF profile management tab

Pure Gas Different Concentration Profile Management

To calibrate the sensor output with different concentrations, the different concentration profile management is implemented, as shown in Figure 5.13. Similar to the pure gas ON/OFF profile management, the user selects the MFC connected to the VOC, the VOC type, the duration, and whether VOC (diluted with nitrogen) or N₂ gas (pure nitrogen) should flow into the chamber. Additionally, this tab allows the user to define a specific VOC concentration for each step.

By clicking “Calculate Flow Rate”, the required VOC and nitrogen flow rates are calculated using Equation E.6 and Antoine coefficients stored in the VOC manager. Afterwards, the step can be added to the profile.

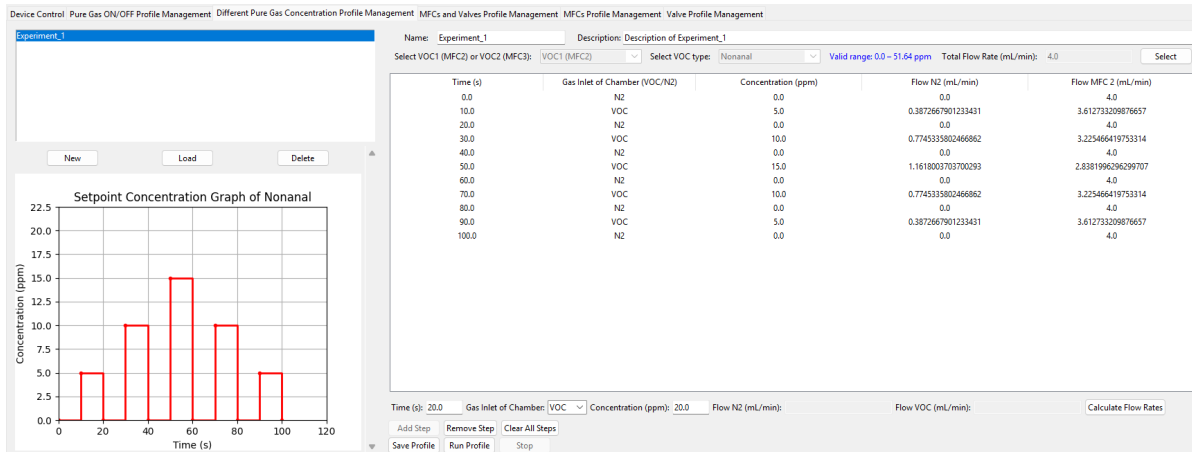


Figure 5.13: Pure gas different concentration profile management tab

In addition to concentration-based profiles, the individual profiles for the devices have also been implemented. These are useful because they allow the user to control and monitor only the MFCs or the valves. Furthermore, the whole setup can also be controlled and monitored without the need to define the concentration.

MFCs Profile Management

The MFCs profile management tab, shown in Figure 5.14, allows users to build time-dependent profiles for the flow rate of all three MFCs. Users can add individual steps by specifying the time and corresponding flow rates for each MFC.

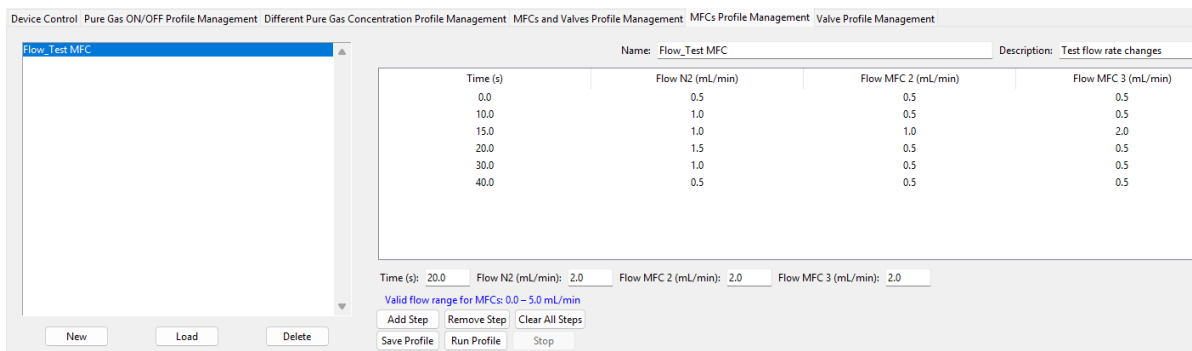


Figure 5.14: MFCs profile management tab

Valve Profile Management

The valve profile management tab, shown in Figure 5.15, allows users to define time-dependent profiles for the two rotary valves. At each step, the desired valve position can be set.

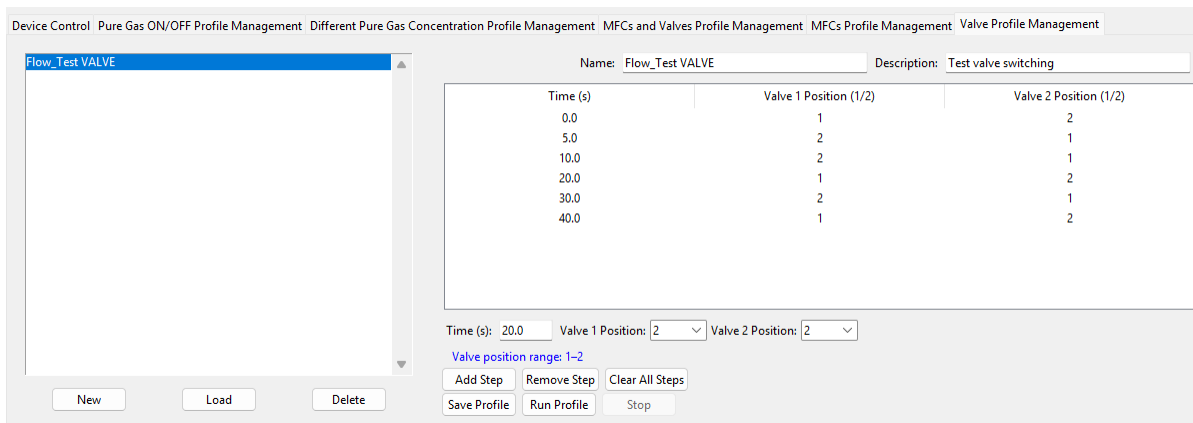


Figure 5.15: Valve profile management tab

MFCs and Valve Profile Management

Finally, the combined MFC and the valve profile management tab, as shown in Figure 5.16 allows users to simultaneously control the flow rates of each MFC and the valves' positions. The user can add steps specifying the time, flow rates for each MFC and the position of the valves without the need to define specific concentrations.

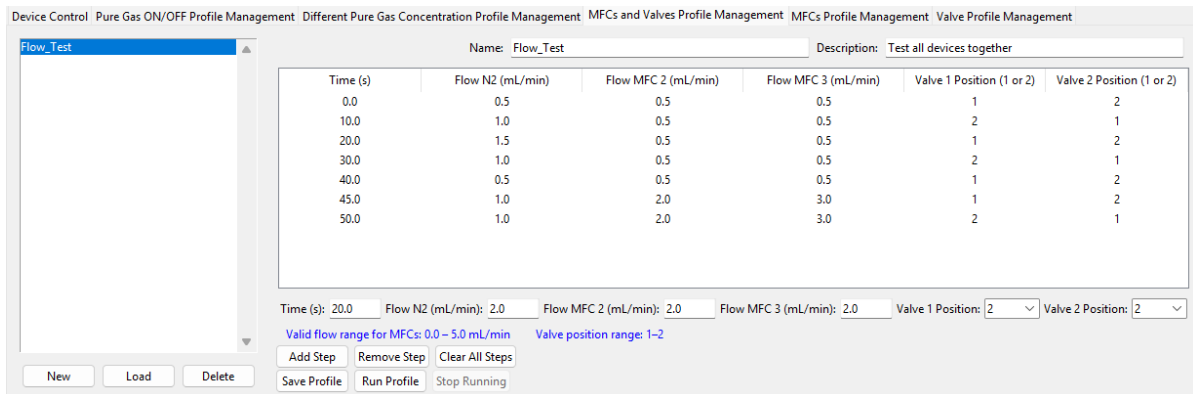


Figure 5.16: MFCs and valve profile management tab

Multiple Profile Runner

Moreover, the multiple profile runner allows users to execute the profile from the MFC profiles tab and the valve profiles tab simultaneously, visualized in Figure 5.17.

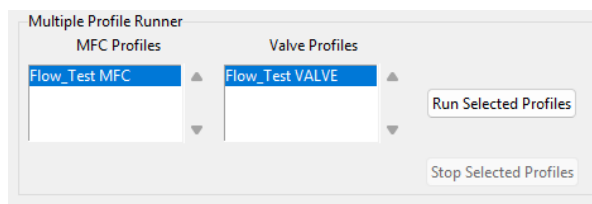


Figure 5.17: Multiple profile runner

6

Discussion

6.1. Socket

The socket successfully replaces the need for screws and allows manual removal from the PCB. This was confirmed through three repeated manual assembly and disassembly during prototyping. However, due to time and equipment constraints, no quantitative measurements of insertion or removal force were performed. The fact that the socket could be inserted and removed by hand indicates that the required force is within an acceptable usage range. Nevertheless, it was observed that a relatively high force was required to remove the barbed rivets. This is likely caused by too many barbs per barbed rivet.

The electrical connection between the QFN-packaged PCS chip and the adapter PCB through an ACS was verified using the continuity test setup in section 5.1. In this test setup, the square frame of the chamber was not been used to press the QFN package against the ACS. This is because once the chamber is placed onto the socket, it becomes impossible to touch the pads of the QFN package. Instead, the test probe was directly pressed to the pads during the measurements. To address this issue in further experiments, a potential solution is to place an intermediate adapter PCB between the current adapter PCB and the sensor board from the previous e-nose system.

6.2. Chamber

Due to limitations in 3D printing accuracy, the chamber was initially not perfectly aligned with the socket. As a result, gas leakage was observed at the interface between the chamber and the socket. This issue was solved by using a PDMS O-ring, which has a low Shore hardness, deforms easily and adapts to uneven surfaces. However, the PDMS-based O-rings are not chemically resistant. When exposed to VOCs such as acetone, they tend to swell, as reported by K.-S. Koh et al. [25]. This will affect the accuracy of the sensor readout. Therefore, it is not suitable for the utilized setup and it has to be replaced later on by a more resilient O-ring material.

The experiment described in section 5.2 shows that there is still some gas leakage in the chamber of approximately 0.07 ml/min. This is within the acceptable margin of error of 0.1 ml/min. This minor leakage was expected, because similar alignment issues are present at the interfaces between the gas tubes and the gas inlet and outlet of the chamber.

Furthermore, the gas leakage of the chamber requires more precise quantification. The current experiment only provides a rough estimate. Flow rates were tested only up to 1.2 ml/min, as higher flow rates made it difficult to count the bubbles accurately. Future experiments could consider using mass flow sensors to more accurately evaluate the performance of the chamber design.

6.3. Automated control system

The mass flow controllers (MFCs) functioned as expected and could be controlled both manually and via the MFC profile management. Although manual serial communication with the valve works reliably, attempts to automate it via the valve profile management were not fully successful. Communication often resulted in incomplete or invalid responses, such as only a single backslash `\` or a fragment as `\0` instead of a full command, such as `\0'2`. This leads to communication errors. Several attempts have been made to resolve this issue, such as increasing the timeout value, which is the time that the system waits until the requested number of bytes is available. Additionally, an extra delay between sending and receiving data was added, yet this issue persisted.

Furthermore, the valve's behavior varies even when running the exact same profile without modifying the code. In some cases, the valve completes the profile successfully. In other cases, the valve returns a half command. This inconsistency suggests that the issue might be related to the valve's internal communication handling, firmware stability, or possibly driver-related problems. It is also possible that timing or structural aspects of the code can contribute to the issue.

Additionally, it has also been observed that profiles with longer delays between valve switching steps tend to produce fewer errors. However, this pattern is still unreliable, as the valve's performance remains inconsistent across runs. Due to time constraints, no further debugging and analysis could be performed.

7

Conclusion

This project focused on the development of three components: the socket, the chamber, and the automated control system. The socket design meets most of the mandatory requirements. It can be attached to the PCB without screws by using barbed rivets. The QFN-packaged PCS chip can be inserted into and removed from the socket using the tweezers holes. Furthermore, an anisotropic conductive sheet (ACS) was used to establish a solderless electrical connection between the chip and the PCB. Continuity tests confirmed electrical connections between the QFN-packaged PCS chip and the ACS. Due to budget constraints, the prototype of the socket was printed in PETG instead of PEEK. Therefore, the prototype does not fully meet the requirement for heat and chemical resistance. This requirement was expected to be fulfilled by using PEEK.

The chamber design meets most of the mandatory requirements. It forms a closed environment around the chip with gas leakage remaining below the acceptable threshold of 0.1 ml/min, as demonstrated in section 5.2. It also includes a gas inlet and outlet that match the dimensions of the gas tubes with an outer diameter of 1/16 inch. Furthermore, using C-shaped sliders as the chamber-socket connection allows the chamber to be frequently removed from the socket. However, due to budget constraints, the chamber prototype was printed in PETG instead of PEEK. As a result, similar to the socket, the prototype does not fully meet the requirement for heat and chemical resistance. This requirement is expected to be fulfilled in the final design by manufacturing the chamber in PEEK.

The automated control system fulfills most of its mandatory requirements. It can communicate via serial ports with the Bronkhorst mass flow controllers (MFCs) and microfluidic rotary valves. Through the developed Python-based graphical user interface (GUI), users can control the flow rates through the MFC and manually set valve positions, as demonstrated in Figure 5.11. Additionally, the system displays real-time data. The system also allows the user to schedule flow rate, valve position and concentration setpoints at specific times and execute those, by the profile management tabs. However, automated valve control via the valve profile, the pure gas ON/OFF profile and the pure gas different concentration profile shows inconsistent behavior. Therefore, [MR.3.5] is only partially fulfilled. In addition to the partially fulfilled mandatory requirements, the trade-off requirements are fulfilled. COM-ports of devices and paths to save custom profiles can be saved. The system can include predefined standard profiles and support new custom profiles. The system also displays the runtime information of the profile when running the profile and visualizes the setpoint graph of the selected concentration profile.

7.1. Recommendations and Future Work

The socket and the chamber were tested using PETG prototypes. In future work, the final design should be printed in PEEK. It should be taken into account that the dimensions and mechanical connection between the socket and the sensor chamber may differ from the PETG version due to the use of a different material and a different 3D printer. As a result, all experimental tests should be repeated to verify the performance of the PEEK implementation. Regarding the barbed rivets, it is recommended to reduce the required insertion and removal force by using fewer barbs per rivet or designing the barbs

with a smaller angle (< 45 degrees). To further verify the required force of the barbed rivets, a tensile testing machine can be used.

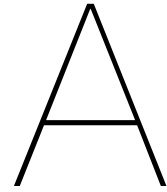
Furthermore, the current prototype chamber uses a PDMS O-ring to prevent gas leakage. However, this type of O-ring is not chemically resistant. Therefore, future work should evaluate alternative chemically resistant O-rings, such as perfluoroelastomer (FFKM).

In addition, the gas temperature in the chamber was not measured in this project. Although short tubing was used to keep the gas temperature consistent after the digital chilling/heating dry bath, it remains an unmonitored variable. Therefore, adding a temperature sensor inside the chamber would allow for more precise thermal control.

Furthermore, the gas concentration is currently estimated based on the Antoine model, which is only theoretically based. To verify the actual VOC concentration inside the sensor chamber. Future work could include sampling the chamber output using a gas chromatography system. This was not tested during the project, as such equipment is not available at TU Delft.

Based on the observed communication issues and the inconsistent behavior of the valve, as explained in section 6.3, further improvements are necessary to ensure stable and reliable operation. To address these issues, it is advised to develop and test profiles with extended delays between the valve switching step, since this reduces the likelihood of communication errors to improve communication stability and ensure reliable valve operation.

Moreover, the automated control system does not yet include the sensor readout system, which is implemented in a separate available MATLAB script. To streamline operation and increase user-friendliness, the readout system needs to be converted to Python and included in the GUI.



Technical drawings

A.1. QFN MLPX5-24-OP01 Package

Figures A.1 to A.4 show the drawings of the QFN MLPX5-24-OP01 package used in this project, as provided by Sempac [9].

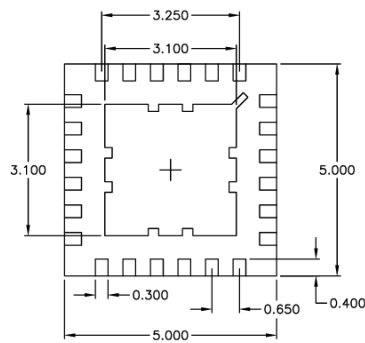


Figure A.1: Bottom view of the QFN package MLP5X5-20-OP-01 [9]

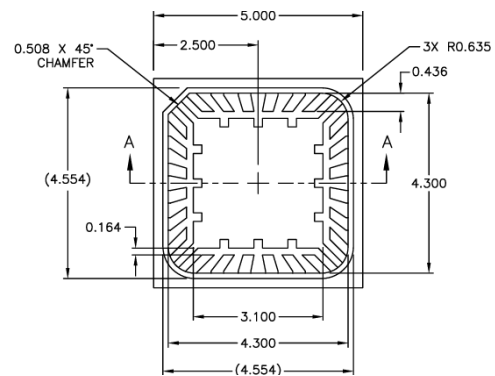


Figure A.2: Top view of the QFN package MLP5X5-20-OP-01 [9]

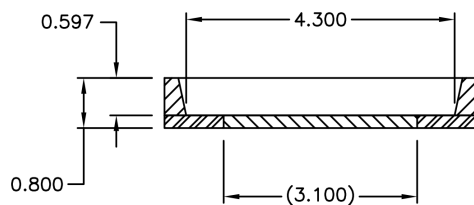


Figure A.3: Cross-sectional view of the QFN package MLP5X5-20-OP-01 [9]

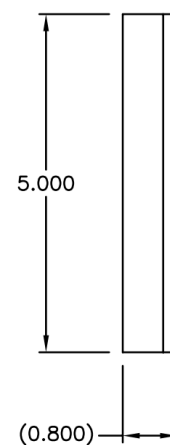


Figure A.4: Side view of the QFN package MLP5X5-20-OP-01 [9]

A.2. Socket

Figure A.5 shows the technical drawings of the designed socket, including the integrated barbed rivets that are part of the design. The same barbed rivet design is also used as a separate component to attach the socket to the PCB. The technical drawings of the barbed rivet are as shown in subsection A.2.1.

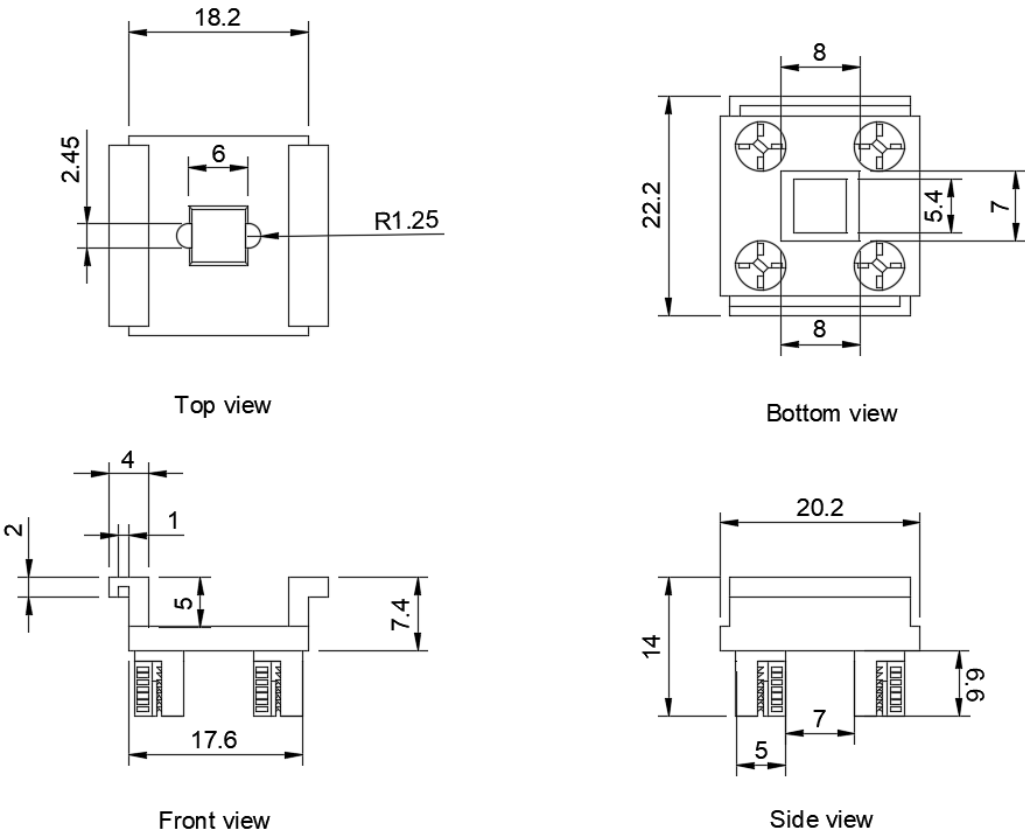


Figure A.5: Technical drawings of the socket

A.2.1. Barbed Rivets

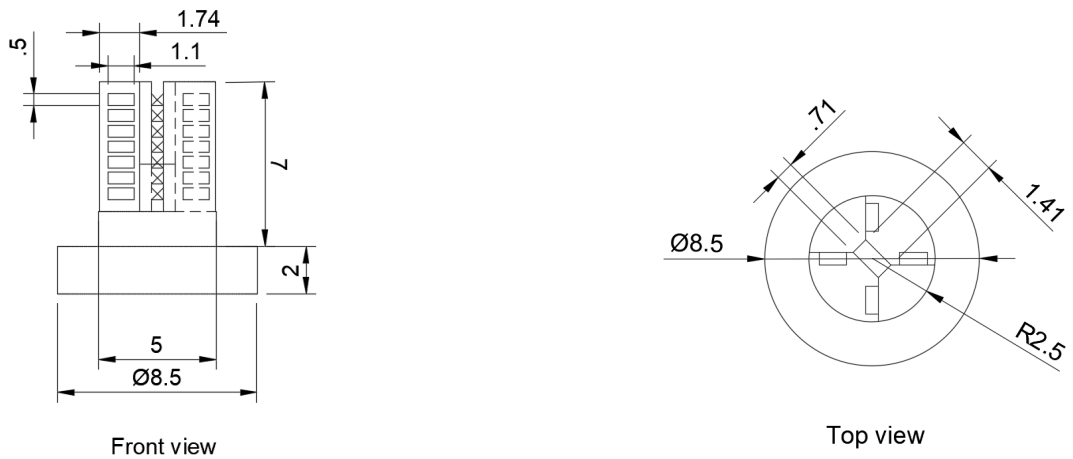


Figure A.6: Technical drawings of the barbed rivet

A.3. Chamber

Figure A.7 shows the technical drawings of the designed chamber.

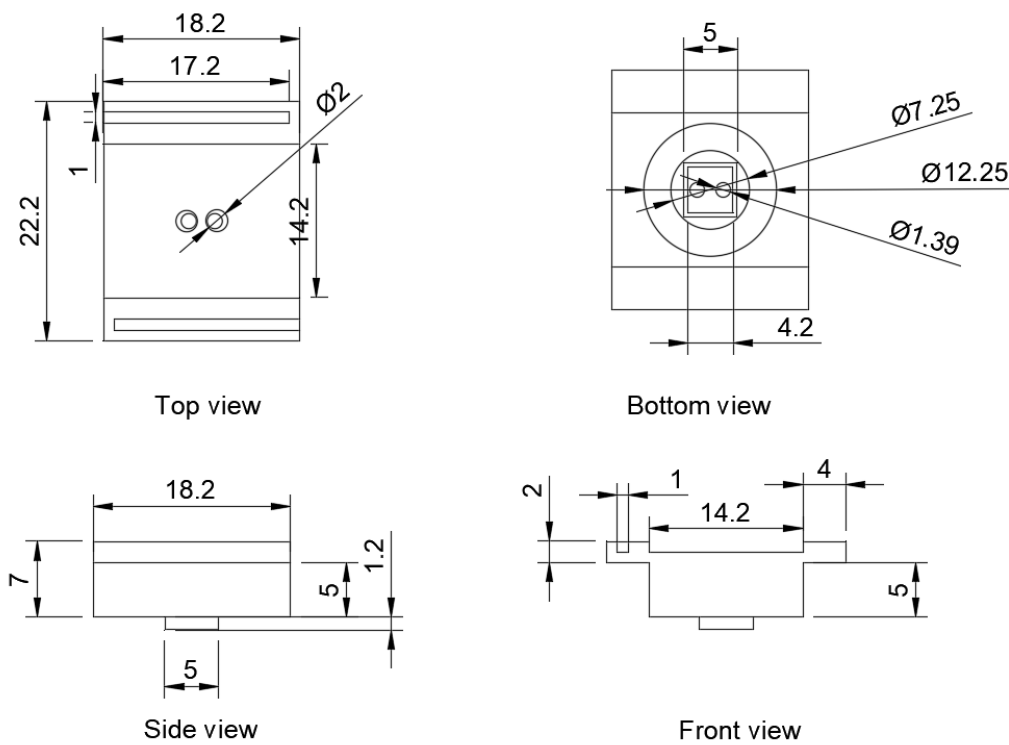


Figure A.7: Technical drawings of the chamber

A.4. C-shaped Slider

Figure A.8 shows the technical drawings of the C-shaped slider.

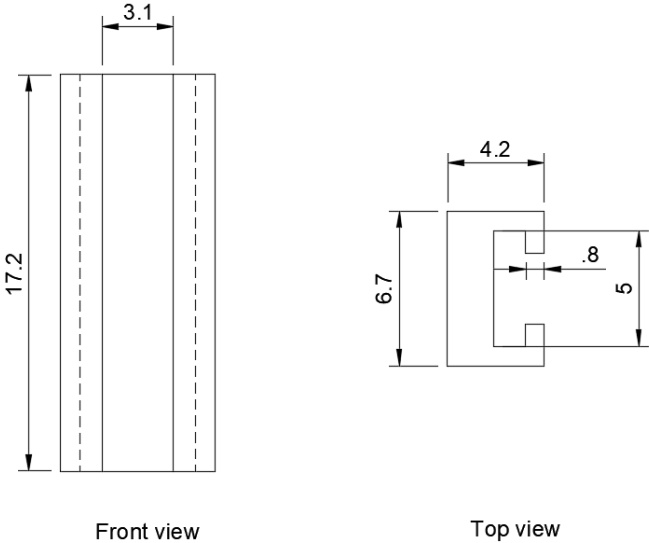


Figure A.8: Technical drawings of the C-shaped slider

B

Socket-PCB connection considerations

B.1. Usage of Rubber

Figure B.1 shows a method that provides a strong mechanical hold due to the frictional resistance of the rubber. However, this approach also makes it more difficult to remove the socket from the PCB. Although the rubber's elasticity allows some flexibility during removal, repeated stretching may lead to tearing over time. Furthermore, it is nearly impossible to find rubber in the exact size and requires shape.

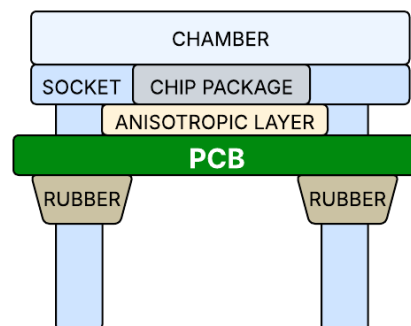


Figure B.1: Socket-PCB usage of rubber side view

B.2. Press-fit

The press-fit mechanism was also considered as a potential socket-PCB connection method. However, this mechanism required high precision and a slightly deformable material. Figure B.2 presents the concept of a single-use press fit, in which the socket is pressed into the PCB. If the shape is exact, this method can provide a strong mechanical hold. The disadvantage is that the mechanical stress may damage the PCB.

Figure B.3 shows an alternative method, where the press-fit occurs between the legs of the socket and a cap. While this design allows for easier removal, it does not provide a strong mechanical hold to keep the socket held in position.

Manufacturing constraints were also taken into account. For example, CNC machining cannot produce a perfectly round shape in aluminium, which poses a challenge for the press-fit designs that rely on high match precision for a tight fit.

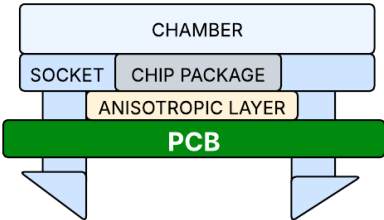


Figure B.2: Socket-PCB single use press-fit side view

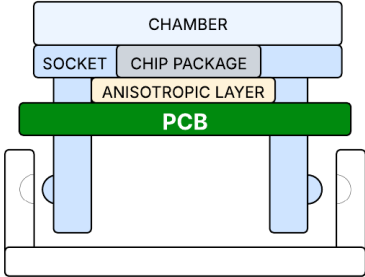


Figure B.3: Socket-PCB press-fit cap side view

B.3. Snap Ring

Another mechanism considered is the snap ring, in which the vertical extensions of the socket that pass through the PCB are fastened using a snap ring, as shown in Figure B.4. This method offers a compact design and allows tool-free attachment and removal. However, because of the small dimensions of the snap ring, it is challenging to attach or remove the ring. Additionally, repeated mechanical stress may lead to material deformation over time.

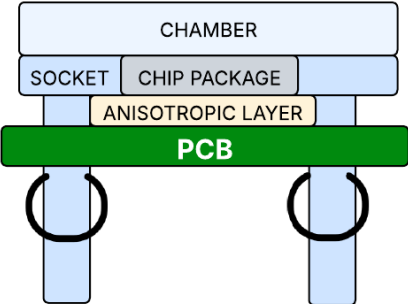
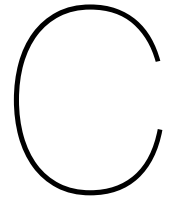


Figure B.4: Socket-PCB snap ring side view



Chamber-Socket connection considerations

C.1. Clamping Mechanisms

An often-used mechanism in socket designs is a clamping mechanism. However, the clamping mechanism introduces mechanical complexity, as they typically require additional components such as springs, screws, or levers. This increases the design's complexity and may reduce its reliability and stability.

C.2. Socket-PCB-Based Fixation

Another method is to rely on the socket-PCB connection to fasten the chamber-socket connection. In this method, the chamber fits tightly into the socket and is held in place indirectly when the socket is mounted onto the PCB. For example, the vertical extensions of the socket can be integrated into the chamber design that extends from the chamber through the aligned holes in the socket and the PCB, as shown in Figure C.1. Once these vertical extensions are fixed to the PCB, the socket and the chamber are firmly held in place. This method offers one connection for the assembly of the chamber, the socket, and the PCB. It ensures that there is proper mechanical pressure and alignment, which contributes to a stable and good connection.

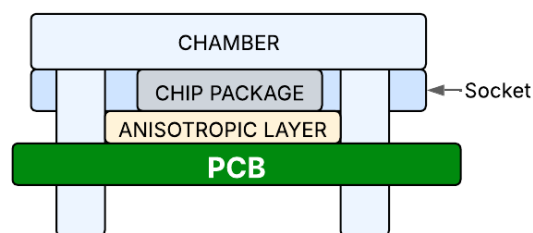
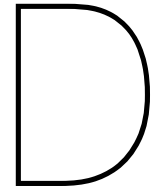


Figure C.1: Socket-PCB based fixation side view

However, this approach is not ideal for applications that require frequent assembly and disassembly. Since the chamber-socket connection depends on the socket-PCB connection, removing the chamber also requires full disassembly of the socket from the PCB. As a result, this design is less practical and user-friendly in cases that require frequent removal of the chamber from the socket.



Flow Characterization in Tubes

D.1. Reynolds Number

The Reynolds number (Re) is used to predict the flow regime of a fluid. The nature of the fluid flow changes depending on the ratio of inertial forces to viscous forces in the fluid, as found by Reynolds [26]. The inertial force is related to the fluid's mass and reflects how difficult it is to change the fluid's speed or direction, which is dominant in fast flows (high Reynolds number). The viscous force is the force required to make a fluid flows and it is dominant in slow flows (low Reynolds number). This relationship can be described by:

$$Re = \frac{\text{inertial force}}{\text{viscous force}} = \frac{\rho D v}{\mu} \quad (\text{D.1})$$

where:

- Re is the Reynolds number
- ρ is the fluid density in kg/m^3
- D is the diameter of the tube in m
- v is the velocity of the fluid in m/s
- μ is the viscosity of the fluid in $\text{Pa} \cdot \text{s}$

The flow pattern can be classified as follows [27]:

- $Re < 2000$: laminar flow, where the gas moves in smooth parallel layers and the flow is stable.
- $2000 < Re < 4000$: transitional flow, where the flow becomes unstable and small disturbances can grow.
- $Re > 4000$: turbulent flow, where the flow is chaotic and unstable.

To relate the Reynolds number to the volumetric flow rate, the fluid velocity is expressed as:

$$v = \frac{V}{A} = \frac{V}{\frac{\pi D^2}{4}} \quad (\text{D.2})$$

where

- v is the velocity of the fluid in m/s
- V is the flow rate in m^3/s
- A is the cross-sectional area of the tube in m^2

- D is the inner diameter of the tube in m

By substituting Equation D.2 into Equation D.1, the following equation is obtained:

$$Re = \frac{4\rho V}{\pi D\mu} \quad (D.3)$$

where:

- Re is the Reynolds number
- ρ is the fluid density in kg/m^3
- V is the flow rate in m^3/s
- D is the diameter of the tube in m
- μ is the viscosity of the fluid in $\text{Pa} \cdot \text{s}$

The inner diameter of the tube used in the experimental setup is 1/32 inch, which corresponds to 0.79375 mm. The volumetric flow rates ranges from 0 to 5 ml/min, equivalent to 0 to $8.33 \times 10^{-8} \text{ m}^3/\text{s}$.

Assuming that the gas in the tube is pure nitrogen at the maximum rate of 5 ml/min. The relevant nitrogen properties at 0 °C is as follows: a dynamic viscosity of nitrogen is $16.63 \times 10^{-6} \text{ Pa} \cdot \text{s}$ from [28], a fluid density is 1.261 kg/m^3 from [29]. Substituting these values in Equation D.3, the obtained Reynolds number is 0.01, which is significantly smaller than the threshold of 2000 for laminar flow.

D.2. Taylor Dispersion

In Appendix D.1, it is explained that the flow inside a tube is laminar when $Re < 2000$. In the setup, laminar flow in the tube is assumed due to the use of a low flow rate and tubes with a small inner diameter. This means that the flow is smooth and follows a parabolic distribution of the flow velocity: the gas flows fastest at the center and slowest near the walls.

When a new gas is introduced into the tube by switching from one gas to another (e.g. from pure nitrogen to VOC1 diluted with nitrogen), due to the parabolic distribution of the flow velocity, the newly introduced gas moves quickly through the center, while some old gas remains near the walls. As a result, a concentration gradient is formed, leading to radial diffusion, which is diffusion perpendicular to the fluid flow.

The combination of parabolic distribution of the flow velocity and the radial diffusion causes the gas to spread along the tube which causes a mix of old and new gases. This phenomenon is known as Taylor dispersion [30]. A schematic overview of the gas flow in a tube illustrating Taylor dispersion is illustrated in Figure D.1, where the newly introduced gas B flows faster through the center than the existing gas A near the walls (black arrows: flow direction, red arrows: radial diffusion). The longer the tube, the more pronounced this effect is. As a result, to minimize this phenomenon, the tubes between the T-connection and the chamber are made as short as possible.

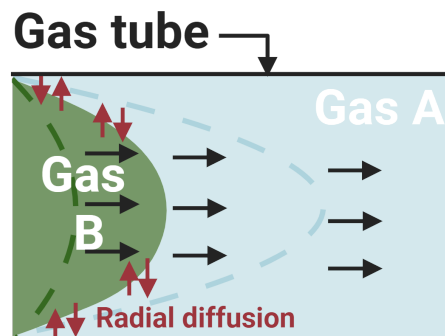
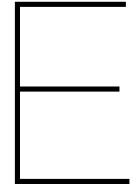


Figure D.1: Schematic overview of the gas flow in a tube illustrating Taylor dispersion



VOC Concentration Calculations

E.1. Flow Rate Equation for Setpoint Concentration

This section derives the equation used to calculate the required flow rates of VOC and nitrogen to achieve a desired target concentration. To determine the correct flow rates for the desired VOC concentrations, the system must first calculate the vapor pressure using the Antoine equation [22]:

$$\log_{10}(P_s) = A - \frac{B}{T + C} \quad (\text{E.1})$$

where

- P_s is the saturated vapor pressure in mmHg
- T is the temperature of the VOC in °C
- A , B and C are Antoine coefficients, which are unique for each substance

This equation can be rewritten to

$$P_s = P_\infty e^{-\frac{T_B}{T+T_C}} \quad (\text{E.2})$$

where

- P_s is the saturated pressure in mmHg
- P_∞ is 10^A , with A being the Antoine coefficient A
- T_B is $B \ln(10)$ in °C, with B being the Antoine coefficient B
- T_C is the Antoine coefficient C in °C
- T is the temperature of the VOC in °C

The Antoine coefficients are obtained for VOCs currently used in the laboratory, as presented in Table E.1. It is important to note that the Antoine equation only holds in thermal equilibrium. Before running each experiment, it is crucial to set the temperature of the VOCs to a stable temperature. In this setup, the digital chilling/heating dry bath is used to manually set the VOC temperature to 0 °C before each experiment. This is to ensure a stable vapor pressure and avoid condensation inside the chamber.

When nitrogen gas is introduced into bottles containing the VOC liquid, it forms bubbles. As these bubbles rise to the surface and burst, they release a gas containing nitrogen and VOC. This VOC-enriched nitrogen stream is then passed through an empty bottle to equalize the pressure before being routed to the rest of the setup. The vapor concentration is determined using Dalton's Law of Partial

Pressures [23]. According to this principle, the partial pressure of a gas component in a mixture is equal to its mole fraction x_{gas} multiplied by the total system pressure:

$$P_s = x_{gas}P \quad (E.3)$$

$$x_{gas} = \frac{P_s}{P} \quad (E.4)$$

In this gas sensing setup, the partial pressure of the VOC corresponds to the saturated vapor pressure P_s , calculated using the Antoine equation. The total system pressure P is assumed to be equal to the atmospheric pressure, i.e. 760 mmHg. This relation allows determining the mole fraction of the VOC vapor x_{gas} . The VOC-enriched nitrogen stream with flow rate f_{VOC} will be diluted with pure nitrogen with flow rate F_{N_2} . The total flow rate becomes equal to $f_{total} = f_{VOC} + F_{N_2}$. Since only a fraction of the VOC-enriched nitrogen stream with flow rate f_{VOC} contains the VOC, the concentration of the VOC can be determined with:

$$C = \frac{P_s}{P} \frac{f_{VOC}}{f_{VOC} + F_{N_2}} \quad (E.5)$$

where

- C is the concentration of the VOC
- f_{VOC} is the flow rate of the VOC- enriched nitrogen stream in ml/min
- F_{N_2} is the flow rate of pure nitrogen gas as a dilution in ml/min

The minimum concentration is 0 ppm, while the maximum concentration is equal to $\frac{P_s}{P}$ where P_s is calculated with Equation E.2. Substituting Equation E.2 into Equation E.5 and rewriting the equation, the required flow rate of the VOC can be determined, which enables automatic control of the MFCs on user-defined concentrations:

$$f_{VOC} = C(f_{VOC} + F_{N_2}) \frac{P}{P_{\infty} e^{-\frac{T_B}{T+T_C}}} = C f_{total} \frac{P}{P_{\infty} e^{-\frac{T_B}{T+T_C}}} \quad (E.6)$$

where

- f_{VOC} is the flow rate of the VOC-enriched nitrogen stream in ml/min
- C is the concentration of the VOC
- F_{N_2} is the flow rate of pure nitrogen gas as a dilution in ml/min
- f_{total} is the total flow rate which is equal to $f_{VOC} + F_{N_2}$
- P_{∞} is 10^A , with A being the Antoine coefficient A
- T_B is $B \ln(10)$ in °C, with B being the Antoine coefficient B
- T_C is the Antoine coefficient C in °C
- T is the temperature of the VOC in °C
- P is the atmospheric pressure of 760 mmHg

Using Equation E.6, the system can determine the corresponding flow rates for the desired VOC concentration.

E.2. Error Margin

A worst-case analysis was performed across the used VOCs in the laboratory, as listed in section 2.2. The nitrogen and VOC flow rates were varied in increments of 0.1 ml/min, while keeping the total flow constant at 5 ml/min. Furthermore, the following inaccuracies were considered to obtain a worst-case analysis based on the specifications of the MFC and the digital chilling/heating dry bath:

- N_2 flow rate F_{N_2} : actual = setpoint – 0.5% of setpoint – 0.1% of 5 ml/min

- VOC flow rate f_{VOC} : actual = setpoint + 0.5% of setpoint + 0.1% of 5 ml/min
- Digital chilling heating dry bath: actual temperature = setpoint (0 °C) + 1°C, due to an accuracy of $\pm 1^\circ\text{C}$.

Using these worst-case conditions, the average deviation in resulting concentration was calculated to be approximately 9.59%. For simplicity and to remain conservative, this is rounded up, and an error margin of 10% is adopted.

E.3. Antoine Coefficients

The Antoine coefficients of Table E.1 are used in combination with Equation E.6 within the Python code to calculate the required flow rates of the VOC and nitrogen to obtain the desired setpoint concentration. The Antoine coefficients and the temperature ranges for these coefficients are primarily from the Iranian Chemical Engineers website [31]. For 1-propanol and 2-propanol, the values are taken from the Chemical Properties Handbook by C.L. Yaws [32].

Table E.1: VOC compounds and corresponding Antoine parameters

VOC compound	A	B (°C)	C (°C)	Tmin (°C)	Tmax (°C)
2-Nonanol	7.87942	1966.54	194.918	-35	349.85
Nonanal	7.42543	1825.65	206.718	-18	366.85
Tetradecane	7.2715	1926.44	187.657	-12.85	418.85
1-dodecanethiol	7.62037	2309.1	212.597	-8	450.85
Ethanol	8.13484	1662.48	238.131	-114.1	243.1
1-Propanol	8.37895	1788.02	227.438	-26	83
2-Propanol	8.87829	2010.33	252.636	-15	98
Methanol	8.09126	1582.91	239.096	-97.68	239.43
Acetone	7.31414	1315.67	240.479	-94.7	235.05
α -Pinene	7.06153	1621.22	231.645	-64	358.85
α -Terpinene	7.13456	1673.54	216.227	-53.15	378.85
1-Butanol	7.62121	1543.89	208.029	-89.3	289.78
Toluene	7.1362	1457.29	231.827	-94.97	318.64
2-Butanone (MEK)	7.29427	1400.37	237.655	-86.67	262.35

3D Rendering of the Adapter PCB Setup

A 3D rendering of the adapter PCB setup is shown in Figure F.1. This figure illustrates the integration of the chamber, socket, and QFN-packaged PCS chip. The chamber with the C-shaped sliders is positioned above the socket. The socket, with an anisotropic conductive sheet beneath it, is placed on the adapter PCB and mechanically fixed with barbed rivets. The adapter PCB is connected to the intermediate PCB via pin headers. This intermediate PCB is connected to the connector socket of the sensing board of the previous e-nose system via pin headers.

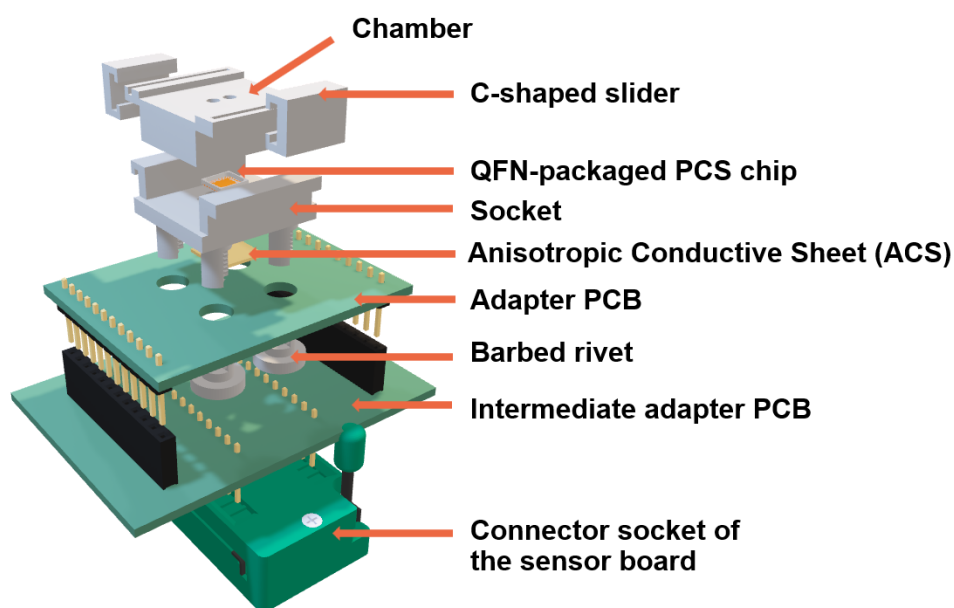


Figure F.1: 3D rendering of the adapter PCB setup

G

The Experimental Setup

G.1. Valve

Figure G.1 shows the physical implementation of the experimental setup used to validate the valve connection and positioning. In the setup, one syringe pumped air using the syringe pumps into the water-filled test tube. By switching between valve positions 1 and 2, the flow paths, and thus the internal connection, were identified, observed through the bubbles formed in the water-filled test tubes.

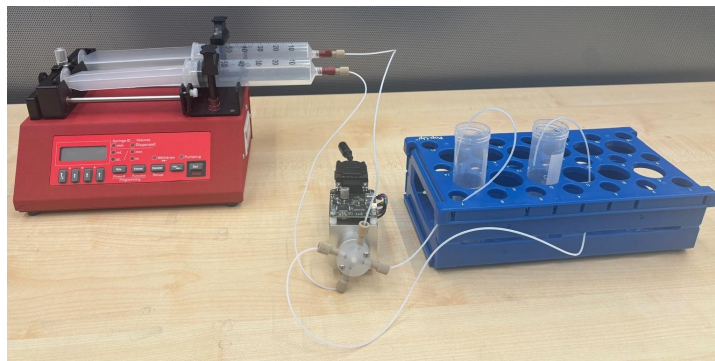


Figure G.1: Valve connection and position validation setup

G.2. Chamber

Figure G.2 shows the physical implementation of the experimental setup used to validate the leakage of the chamber. Air was pumped through two syringes using the syringe pump. One syringe directed air into a test tube filled with water via the chamber, while the other syringe delivered air directly into the second test tube filled with water. The number of bubbles generated in the test tubes was compared over time. Any significant discrepancy would indicate a leak in the chamber.

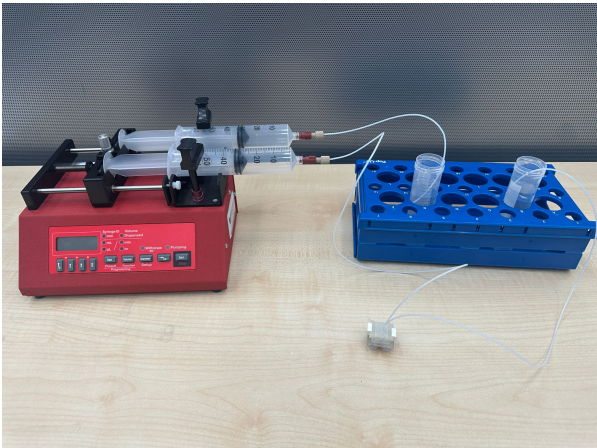


Figure G.2: Chamber leakage experimental setup

Bibliography

- [1] L. Cheng, M. Q., A. Lilienthal, and P. Qi, "Development of compact electronic noses: A review," *Measurement Science and Technology*, vol. 32, no. 6, p. 062 002, 2021, ISSN: 0957-0233. DOI: 10.1088/1361-6501/abef3b. [Online]. Available: <https://doi.org/10.1088/1361-6501/abef3b>.
- [2] Ironwood Electronics, *Ironwood electronics catalog 23*, 2010. [Online]. Available: https://www.bce.it/wp-content/uploads/2012/02/Ironwood_catalog_23_small.pdf.
- [3] P. Borowik, T. Grzywacz, R. Tarakowski, *et al.*, "Development of a low-cost electronic nose with an open sensor chamber: Application to detection of *ciboria batschiana*," *Sensors*, vol. 23, no. 2, 2023. DOI: 10.3390/s23020627. [Online]. Available: <https://www.mdpi.com/1424-8220/23/2/627>.
- [4] Q. Xu, Y. Su, L. Sun, and J. Cai, "Detection of citrus huanglongbing at different stages of infection using a homemade electronic nose system," *Computers and Electronics in Agriculture*, vol. 229, p. 109 845, 2025. DOI: <https://doi.org/10.1016/j.compag.2024.109845>. [Online]. Available: <https://www.sciencedirect.com/science/article/pii/S0168169924012365>.
- [5] N. Samiyan and M. Addi, "Characterization of sensing chamber design for e-nose applications," *Journal of Telecommunication, Electronic and Computer Engineering*, vol. 9, pp. 123–127, 2017. [Online]. Available: <https://api.semanticscholar.org/CorpusID:139515782>.
- [6] Z. Wu, F. Tian, J. A. Covington, *et al.*, "Triplet calibration for general-purpose electronic noses," *Microchemical Journal*, vol. 209, p. 112 652, 2025. DOI: 10.1016/j.microc.2025.112652. [Online]. Available: <https://doi.org/10.1016/j.microc.2025.112652>.
- [7] F. Widdershoven, "Pixelated capacitive sensors (pcs) for embedded multi-sensing," in *Imaging Sensors, Power Management, PLLs and Frequency Synthesizers: Advances in Analog Circuit Design 2023*, K. A. A. Makinwa, A. Baschiroto, and B. Nauta, Eds. Cham: Springer Nature Switzerland, 2025, pp. 23–35, ISBN: 978-3-031-71559-4. DOI: 10.1007/978-3-031-71559-4_2. [Online]. Available: https://doi.org/10.1007/978-3-031-71559-4_2.
- [8] Intech Technologies, *What is IC packaging; Why is it important?* Apr. 2024. [Online]. Available: <https://intech-technologies.com/what-is-ic-packaging-why-is-it-important/#:~:text=The%20most%20obvious%20importance%20of, reliable%20in%20diverse%20operating%20conditions..>
- [9] Sempac, *MLP5X5-24-OP-01 Open Cavity Plastic Package - QFN Package - Open-Pak*, 2021. [Online]. Available: <https://europactice-ic.com/wp-content/uploads/2019/06/MLP5X5-24-OP-01-1-R2-ECN-10492.pdf>.
- [10] Aalco Metals Ltd, *Aluminium alloy 6061 - t6 extrusions*, n.d. [Online]. Available: https://www.aalco.co.uk/datasheets/Aalco-Metals-Ltd_Aluminium-Alloy-6061-T6-Extrusions_145.pdf.ashx.
- [11] INTAMSYS, *Intamsys® peek technical data sheet v3*, 2025. [Online]. Available: https://143787771.fs1.hubspotusercontent-eu1.net/hubfs/143787771/Filament_Datesheet/INTAMSYS_PEEK_TDS_V3.pdf.
- [12] Industrial Specialties Mfg. and IS MED Specialties, *Aluminum chemical compatibility chart*, n.d. [Online]. Available: <https://www.industrial-spec.com/images/files/aluminum-aluminium-chemical-compatiblity-chart-from-ism.pdf>.
- [13] Zeus Company LLC, "Chemical compatibility of PEEK," Tech. Rep. [Online]. Available: <https://www.zeusinc.com/wp-content/uploads/2022/03/PEEK-Chemical-Compatibility-Chart-V1R1.pdf>.

- [14] P. Olyslaegers and Y. Machtane, "Mixed signal pcb design and analog readout circuitry for a pixelated capacitive sensor e-nose array," Bachelor's thesis, Delft University of Technology, Jun. 2025.
- [15] H. Tomozawa, *What is ACF (Anisotropic Conductive Film)? Its usages, how to apply, types, and more are explained*. 2023. [Online]. Available: <https://www.resonac.com/solution/tech/acf.html>.
- [16] ShinEtsu, *MT-Type*, n.d. [Online]. Available: <https://shinpoly.com/mt-type/>.
- [17] Texas Instruments, *Pcb design guidelines for reduced emi*, <https://www.ti.com/lit/an/szza009/szza009.pdf>, 1999.
- [18] F. Annanouch, G. Bouchet, P. Perrier, *et al.*, "How the chamber design can affect gas sensor responses," *Proceedings*, vol. 2, p. 820, Nov. 2018. DOI: 10.3390/proceedings2130820.
- [19] Bronkhorst®, "Instruction Manual Operational Instructions for Digital Multibus Mass flow / Pressure Instruments," Tech. Rep., 2025. [Online]. Available: <https://prod-bronkhorst-products-cdn-cdwbfhmd0gfecfb.a02.azurefd.net/media/prqhjq5u/917158-manual-flexi-flow-compact.pdf>.
- [20] Torrey Pines Scientific, Inc, "OPERATING MANUAL EchoTherm DIGITAL, ELECTRONIC CHILLING/HEATING DRY BATH MODELS IC20, IC20XR, IC20XT, IC30, IC30XR, and IC30XT," Tech. Rep., 2021. [Online]. Available: https://torreypinespro.wpenginepowered.com/download/58/digital-dry-baths-bench-top/20139/man-ic20v5-xt-xr-ic30-xt-xr_feb_2021.
- [21] Advanced Microfluidics SA, *Operating Manual RVM Rotary valve*. 2023. [Online]. Available: <https://amf.ch/app/uploads/2023/09/AMF-RVM-Industrial-Microfluidic-Rotary-Valve-Operating-Manual.pdf>.
- [22] C. Antoine, "Tensions des vapeurs: Nouvelle relation entre les tensions et les temperatures," *Comptes Rendus des Séances de l'Académie des Sciences*, vol. 107, pp. 681–684, 778–780, 836–837, 1888.
- [23] J. Dalton, "Essay IV. On the expansion of elastic fluids by heat," *Memoirs of the Literary and Philosophical Society of Manchester*, vol. 5, no. 2, pp. 595–602, 1802.
- [24] MatWeb, LLC, *Ptfe material properties overview*. [Online]. Available: https://www.matweb.com/search/datasheet_print.aspx?matguid=4e0b2e88eeba4aaeb18e8820f1444cdb.
- [25] K.-S. Koh, J. Chin, J. Chia, and C.-L. Chiang, "Quantitative studies on pdms-pdms interface bonding with piranha solution and its swelling effect," *Micromachines*, vol. 3, no. 2, pp. 427–441, 2012. [Online]. Available: <https://www.mdpi.com/2072-666X/3/2/427>.
- [26] O. Reynolds, "An experimental investigation of the circumstances which determine whether the motion of water shall be direct or sinuous, and of the law of resistance in parallel channels," *Proceedings of the Royal Society of London*, vol. 35, pp. 84–99, 1883. DOI: 10.1098/rsp1.1883.0018.
- [27] M. Saldana, S. Gallegos, E. Gálvez, *et al.*, "The Reynolds Number: A Journey from Its Origin to Modern Applications," *Fluids*, vol. 9, no. 12, p. 299, 2024. DOI: 10.3390/fluids9120299. [Online]. Available: <https://doi.org/10.3390/fluids9120299>.
- [28] Engineeringtoolbox, *Nitrogen - Dynamic and Kinematic Viscosity vs. Temperature and Pressure*, n.d. [Online]. Available: https://www.engineeringtoolbox.com/nitrogen-N2-dynamic-kinematic-viscosity-temperature-pressure-d_2067.html.
- [29] Engineeringtoolbox, *Nitrogen (N2) Density and Specific Weight: Temperature and Pressure data and calculator*, n.d. [Online]. Available: https://www.engineeringtoolbox.com/nitrogen-N2-density-specific-weight-temperature-pressure-d_2039.html.
- [30] G. I. Taylor, "Dispersion of soluble matter in solvent flowing slowly through a tube," *Proceedings of the Royal Society of London A Mathematical and Physical Sciences*, vol. 219, no. 1137, pp. 186–203, 1953. DOI: 10.1098/rspa.1953.0139. [Online]. Available: <https://doi.org/10.1098/rspa.1953.0139>.

-
- [31] Iranian Chemical Engineers Website, *ANTOINE COEFFICIENTS FOR VAPOR PRESSURE*, n.d. [Online]. Available: http://catalysis.eprints.iitm.ac.in/3012/1/ANTOINE_COEFFICIENTS_FOR_VAPOR_PRESSURE%5B1%5D%5B4619259%5D.PDF.
- [32] C. L. Yaws, *Chemical Properties Handbook*. New York: McGraw-Hill Education, 1999.